Petroleum Science 21 (2024) 2502–2519

Contents lists available at ScienceDirect

Petroleum Science

journal homepage: www.keaipublishing.com/en/journals/petroleum-science

Original Paper

Study of inter-well interference in shale gas reservoirs by a robust production data analysis method based on deconvolution

Wen-Chao Liu [a, *], Cheng-Cheng Qiao [a], Ping Wang [b], Wen-Song Huang [b], Xiang-Wen Kong [b], Yu-Ping Sun [b], He-Dong Sun [b], Yue-Peng Jia [b]

[a] School of Civil and Resource Engineering, University of Science and Technology Beijing, Beijing, 100083, PR China
[b] PetroChina Research Institute of Petroleum Exploration and Development, Beijing, 100083, PR China

ARTICLE INFO

Article history:
Received 13 August 2023
Received in revised form
6 March 2024
Accepted 7 March 2024
Available online 8 March 2024

Edited by Yan-Hua Sun

Keywords:
Shale gas
Inter-well interference
Deconvolution
Production data analysis
Typical curves
Multi-stage fractured horizontal well

ABSTRACT

In order to overcome the defects that the analysis of multi-well typical curves of shale gas reservoirs is rarely applied to engineering, this study proposes a robust production data analysis method based on deconvolution, which is used for multi-well inter-well interference research. In this study, a multi-well conceptual trilinear seepage model for multi-stage fractured horizontal wells was established, and its Laplace solutions under two different outer boundary conditions were obtained. Then, an improved pressure deconvolution algorithm was used to normalize the scattered production data. Furthermore, the typical curve fitting was carried out using the production data and the seepage model solution. Finally, some reservoir parameters and fracturing parameters were interpreted, and the intensity of inter-well interference was compared. The effectiveness of the method was verified by analyzing the production dynamic data of six shale gas wells in Duvernay area. The results showed that the fitting effect of typical curves was greatly improved due to the mutual restriction between deconvolution calculation parameter debugging and seepage model parameter debugging. Besides, by using the morphological characteristics of the log-log typical curves and the time corresponding to the intersection point of the log-log typical curves of two models under different outer boundary conditions, the strength of the interference between wells on the same well platform was well judged. This work can provide a reference for the optimization of well spacing and hydraulic fracturing measures for shale gas wells.

1. Introduction

Due to cost constraints, shale gas reservoirs typically rely on platform-based deployment of horizontal wells, factory drilling and fracturing, and sustained large-scale operations to achieve economic development. To prevent the possible negative outcome of reduced output from new wells due to interference from infill drilling and fracturing operations, the shale gas well network and well spacing must be optimally deployed at the initial stage (Wei et al., 2018). As shown in Fig. 1. In infill drilling operations, the interference between adjacent wells will affect the completion of the well, especially the fracture propagation (Al-Shami et al., 2023). Studies have shown that areas with well-developed natural fracture-fracture networks are more susceptible to interference and fracture channeling occurs between or within the well group platforms (Ge et al., 2022). Meanwhile, substantial inter-well interference can arise when all adjacent wells on the same platform produce simultaneously. Therefore, it is essential to ensure the appropriateness of the deployment of well pattern and well spacing at once. If the well spacing is too extensive, the inter-well reservoir may be challenging to activate effectively through volume fracturing. On the contrary, inadequate well spacing can lead to severe inter-well interference (Paryani et al., 2017; Gupta et al., 2020; Chen et al., 2021). Both will affect the mining efficiency. Hence, maintaining a balance between avoiding significant inter-well interference due to inadequate well spacing and maximizing the utilization efficiency of reservoirs is pivotal to enhance the economic benefits of shale gas reservoir development.

Dynamic production data analysis method is one of the most important means for the dynamic description of shale gas reservoirs. It combines the advantages of well test analysis and gas

* Corresponding author
E-mail addresses: wcliu_2008@126.com, b1701026@ustb.edu.cn (W.-C. Liu).

https://doi.org/10.1016/j.petsci.2024.03.003

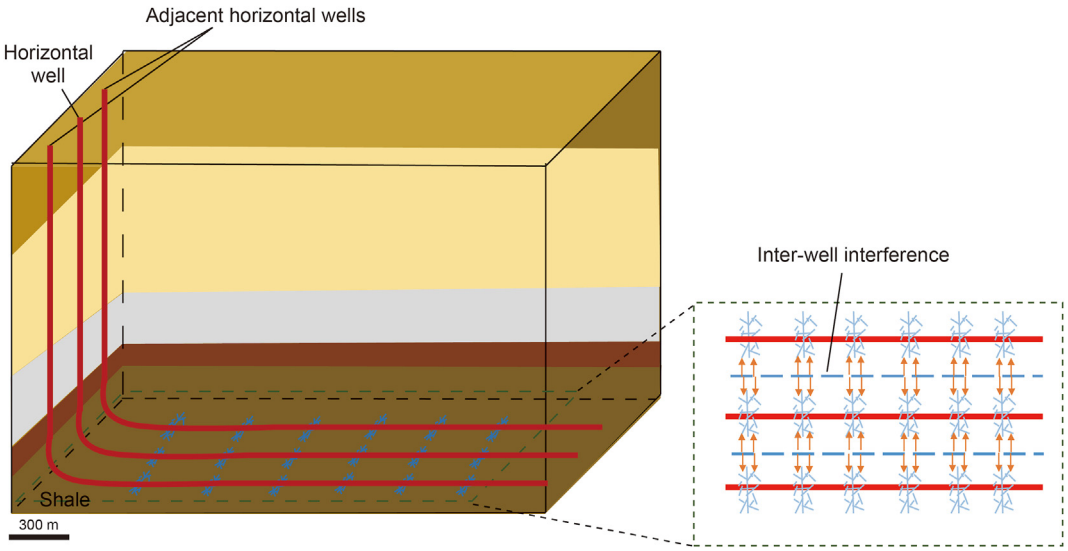

Fig. 1. Diagram of inter-well interference of multi-stage fractured horizontal wells in shale gas reservoirs (modified from Al-Shami et al., 2023).

reservoir engineering. Parameters such as reservoir permeability, fracture length, fracture conductivity and well recoverable reserves can be obtained by processing and analyzing production data. It can provide a strong technical guarantee to enhance the development efficiency and reduce the risk of shale gas reservoirs by detecting inter-well interference effects and predicting gas well production declines. The method has the characteristics of practicality, reliability and cost-effectiveness (Villarreal and Moghanloo, 2022). Due to the important role of dynamic production data analysis in shale gas reservoirs exploitation, many methods have been proposed by predecessors. The first method is the traditional production decline analysis method (Sharma et al., 2019). Gupta et al. (2018) proposed a new, simplified decline curve equation to predict the productivity of shale gas in the Haynesville and Eagle Ford formations by modifying the existing Arps exponential decline equation. Additionally, a hybrid approach was developed to predict shale gas recoverable reserves in the Weiyuan Block of the Sichuan Basin through a combination of stretch exponential production-decline and an improved Duong's method (Wang et al., 2020). However, the models used in these methods often rely on empirical formulas and lack sufficient theoretical basis. Moreover, only production prediction can be made, and prediction accuracy is also greatly affected by various factors such as geological conditions, development schemes, production well types. These models cannot effectively identify the unique characteristics of hydraulic fractures and reservoir parameters. Furthermore, the early production of shale gas tends to decline significantly, and the production status can be quite unstable. Because of these challenges, the traditional production decline analysis method has limited applicability for shale gas reservoirs. The second method is the dynamic production data analysis method based on artificial intelligence (Ma et al., 2018; Liu et al., 2021). Xiao et al. (2022) proposed an efficient and robust post-history production forecasting framework using a latent-space learning-based direct forecast approach; it has a good effect on the productivity prediction of fractured shale reservoirs. Two linear and nonlinear hybrid artificial intelligence prediction methods were developed to predict shale gas production in Pennsylvania and Texas (Wang and Jiang, 2019); the results showed that the growth rate of shale gas production in Pennsylvania was higher than that in Texas in 2017 and 2018. He et al. (2023) established a shale gas production evaluation system based on data-driven models to predict shale gas production. The accuracy of production prediction can reach more than 95%. Meng et al. (2023) proposed a multi-well data-driven framework. By using it to analyze shale gas production data, suggestions for increasing production are provided. In general, the dynamic production data analysis method based on artificial intelligence can solve the tough problem of complex production data processing and also improves the reliability of the results. However, it ignores the internal relationship between the input feature data, and cannot fully extract the feature information. It is also difficult to figure out which is the main factor affecting production capacity. In addition, the dynamic production data analysis method based on artificial intelligence also needs a sufficient amount of learning samples. The third method is typical curve analysis. Some scholars (Shi et al., 2020; Zhang and Meybodi, 2020; Zeng et al., 2021) analyzed the flow regime by establishing linear flow models to fit dynamic production data; the product of the half length of fracture and the half power of matrix permeability can be calculated according to the slope of the log-log typical curves of flow rate at a specific flow state. Lu et al. (2019) proposed a semi-analytical Blasingame decline analysis model. This model incorporates multi-flow mechanisms and modified material balance pseudo time for more accurate analysis of shale reservoirs. In addition, this study suggests a research method to investigate the impact of factors such as hydraulic fracture properties, gas desorption, and gas diffusion on production decline using Blasingame typical curves. Ren and Lau (2020) developed a quad-linear flow model for multi-stage fractured horizontal wells in shale gas reservoirs by taking into account secondary fractures that form around hydraulic fractures. The model was validated using production data from two wells, and sensitivity analysis of the uncertainty parameters was conducted to identify factors affecting production capacity. Xu et al. (2021) developed a semi-analytical model for shale gas reservoirs developed by hydraulically fractured wells. The model utilized the wellbore pressure derivative curve and Blasingame production decline integral derivative curve to classify various flow regimes and analyze the characteristics of different flow types. Cui et al. (2022) developed a semi-analytical model for a multi-horizontal well pad with damaged fractures. By using numerical inversion techniques, typical pressure derivative curves were obtained, and the effects of critical parameters on transient pressure were

studied; the results indicated that pressure derivative curves increase gradually under inter-well interference. Wang et al. (2018) proposed a semi-analytical method to simulate the pressure interference response in multi-well pad. To verify the reliability of the new model, the researchers applied it to a multi-well platform comprising six wells in South China. The results confirmed the validity of the model and its potential for practical field development. In summary, the typical curve analysis method is commonly used in petroleum engineering, despite its high requirements for model selection. However, the above studies have shown that there is still limited research on dynamic production data analysis for shale gas reservoirs, particularly methods for analyzing multi-well interference. This can be attributed to the unique seepage mechanisms and complex development patterns in tight shale formations. Existing mathematical models for studying multi-well interference in shale gas reservoirs tend to be highly complicated, which further deter research progress in this area. What's more, the production data of shale gas has relatively large errors, and the pressure and production rate data are seriously fluctuated. As a result, most of the existing multi-well models are still at the theoretical level and lack of application to actual field cases.

As previously mentioned, the flow dynamics of shale gas reservoirs during production are highly variable, with field-measured production rates and pressures of horizontal wells constantly changing over time. However, mathematical models used for the analysis of production data typically assume internal boundary conditions of constant flow rate or constant production pressure. In conventional reservoir development techniques, well shut-in testing techniques are commonly used to solve the problem of mismatch between boundary conditions within an ideal mathematical model and field data. Unfortunately, for unconventional shale gas reservoirs, well shut-in tests may significantly impact shale gas production and lead to significant economic losses due to the extremely low reservoir permeability and the high cost of hydraulic fracturing measures. It is often easier to obtain production data than well test data, but the accuracy of production data is often lower. Using raw production data directly can result in a scattered distribution of typical data points and lead to limited investigation scope for production data analysis. Consequently, relying on raw data alone can lead to a large degree of uncertainty in data fitting. Although the conventional method of combining rate normalized pressure with superposition time (Liang et al., 2017; Clarkson et al., 2020) can convert pressure under variable flow rate conditions to pressure under constant flow rate. However, it is only effective for steady-state or slowly varying production rate and flow pressure data over time. As such, it cannot effectively convert production data with abrupt or discontinuous changes for unconventional reservoirs. Fortunately, deconvolution based on Duhamel's principle as a useful tool can avoid the limitations of traditional normalization methods. It can convert raw production data from shale gas reservoirs into bottom hole flowing pressure per unit flow rate, which is an approach that effectively matches the inner boundary conditions of interpretation models. Unlike traditional methods, deconvolution can also eliminate the effect of data errors, suppress data divergence, and expand the scope of investigation for interpretation. After more than 40 years of the research, the pressure deconvolution algorithm has been mature. Representative deconvolution algorithms include von Schroeter algorithm (von Schroeter et al., 2004), ILK algorithm (Ilk et al., 2006), their improved algorithms (Liu et al., 2018) and data-driven deconvolution algorithm (Pan et al., 2020). In addition, for the current multi-well production mode, many multi-well deconvolution algorithms have been proposed, which can remove the effect of well interference. For example, Cumming et al. (2014) proposed a new method for multi-well deconvolution by vectorizing the single-well deconvolution problem as framed by von Schroeter et al. (2004). Jaffrezic et al. (2019) used pseudo-time to extend the application of constrained multi-well deconvolution algorithm to gas reservoirs with significant pressure depletion. Afanaskin et al. (2022) proposed a specially modified CRM-model (capacitance resistive model) for multi-well deconvolution in carbonate reservoirs to assess inter-well interference and to determine the inter-well seepage flow capacity. As pressure deconvolution algorithms continue to be optimized, their application in unconventional reservoir engineering becomes increasingly practical. This development has greatly facilitated the progress of well testing and dynamic production data analysis. However, when processing actual field data from shale gas reservoirs that may be subject to pressure and flow rate data noise, most multi-well deconvolution algorithms remain subject to significant uncertainty. The success of these algorithms is largely determined by the quality of pressure and flow rate data, requiring high-resolution dynamic production data. As a result, applying multi-well deconvolution algorithms to large-scale production dynamic data analysis of shale gas wells has proven challenging.

In this paper, a new robust production data analysis method for studying inter-well interference in shale gas reservoirs was proposed based on pressure deconvolution algorithm. Firstly, a multi-well conceptual model was proposed to describe the seepage flow process of shale gas reservoirs considering inter-well interference and its Laplace solutions under two different outer boundary conditions were given. Secondly, the improved pressure deconvolution algorithm was used to normalize large amount of dynamic production data. Thirdly, the adjustment of normalization parameters of deconvolution calculation and the adjustment of model parameters of mathematical model were mutually restricted. Then, the log-log typical curves of pseudo pressure drop and pseudo pressure drop derivative calculated by the normalized dynamic production data were fitted with the ones calculated by the mathematical model with constant production rate. Finally, the strength of the inter-well interference of shale gas multi-stage fractured horizontal wells on the same well platform was judged by using the convergence speed of the log-log typical curves in the later period and the time corresponding to the intersection point of the log-log typical curves under different outer boundary conditions. This study greatly improves the fitting effect of the typical curves. It can quickly and accurately interpret fracture parameters (fracture conductivity, fracture half-length, etc.) and reservoir parameters (outer boundary distance, permeability, porosity, recoverable reservoirs of shale gas, etc.). The proposed method has important practical significance as it could provide valuable technical support for implementing stimulation measures, as well as predicting production decline.

2. Dynamic production data analysis of shale gas reservoirs based on deconvolution algorithm

2.1. Multi-well seepage model of multi-stage fractured horizontal wells in shale gas reservoirs

Considering the zonal flow characteristics of shale gas in shale reservoirs with multi-stage fractured horizontal well inter-well interference, a multi-well conceptual model of shale gas reservoirs was established, as shown in Fig. 2. The physical model consists of horizontal wells, main fractures and shale reservoir. The shale reservoir is extremely tight, and then it can be considered reasonably that the inter-well interference only exists between adjacent wells. Due to the interference between adjacent wells, outer boundaries equivalent to the closed boundary are formed, as shown in red horizontal dotted lines in Fig. 2. No fluid flows at the

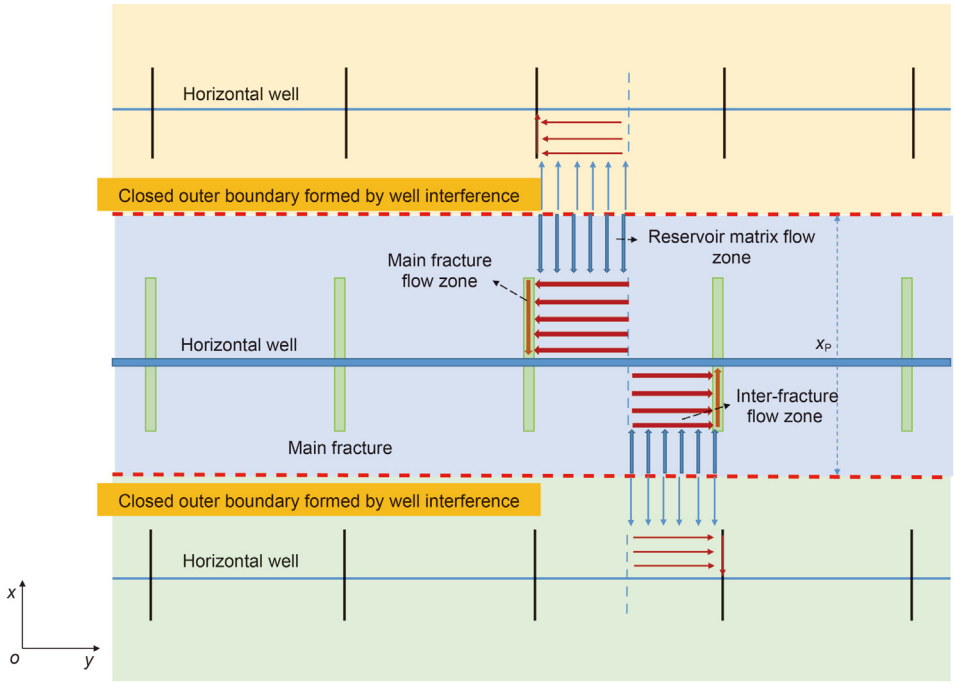

Fig. 2. Multi-well conceptual physical model of shale gas reservoirs.

closed outer boundaries. After each well is disturbed by adjacent wells, a sphere of influence is formed around the well, as shown in Fig. 2 with different colored shaded areas. Assuming that the formed potential is uniform, so it is considered that the outer boundary distances on both sides of each well are equal. Twice the outer boundary distance is the range of the potential formed by the interference between wells, represented by x_p in Fig. 2. Assuming that the closed outer boundary is fixed, and the proposed conceptual model is suitable for cases where the producing pressure drop conditions of adjacent wells remain roughly the same such as for adjacent wells on the same platform. The reasonableness of the assumption that the closed outer boundary can be set as fixed is explained in Appendix A. The conclusion in practical application part also supports the assumption.

The seepage flow characteristics of shale gas affected by inter-well interference are analyzed. Since the production period of multi-stage fractured horizontal wells is mainly governed by linear flow, by assuming the same hydraulic fracture is uniformly distributed along the horizontal well length, the complex flow process of shale gas in reservoirs can be simplified as linear flow in three adjacent flow zones: main fracture flow zone, inter-fracture flow zone and reservoir matrix flow zone (Brown et al., 2011). That is, shale gas flows from the reservoir matrix flow zone to the inter-fracture flow zone, and then flows to the main fracture flow zone, and finally flows to the wellbore. It is worth noting that shale gas mainly exists in organic-rich shale in the form of free gas and adsorbed gas. Prior experience with shale gas production indicates that the early stage of production mainly involves shale gas coming from fractures and well-connected free gas. However, at the middle and later stages of production, shale gas is mainly sourced from the desorption of adsorbed gas found in mesopores and micropores of organic matter (Xiong et al., 2022). Considering the adsorption and desorption of shale gas reservoirs (Alafnan et al., 2021), mathematical models for the flow in the three zones (Brown et al., 2011) are established respectively. The model does not specifically consider the confinement effect in nano-micron pores of shale matrix (Du and Nojabaei, 2020), and the permeability of matrix can be considered as the homogenized apparent permeability. Main fractures are assumed to have the same properties, equal spacing along the horizontal well direction and equal fracture length. Furthermore, the model does not take into account the flow within horizontal wells. In other words, horizontal wells are assumed to be infinitely conductive.

Based on the established shale gas multi-well conceptual model, a traditional three-linear seepage model with closed outer boundary conditions in the reservoir matrix flow zone is introduced to characterize the shale gas seepage flow process with inter-well interference. Then, the dimensionless pseudo bottom hole flowing pressure solution corresponding to the constant flow rate considering the skin effect is obtained by Laplace transform (Brown et al., 2011):

$$\tilde{m}_{\mathrm{wD}} = \frac{k_{\mathrm{I}} x_{\mathrm{F}}}{2 k_{\mathrm{F}} w_{\mathrm{F}} s \sqrt{\alpha_{\mathrm{F}}} \tanh\left(\sqrt{\alpha_{\mathrm{F}}}\right)} + \frac{k_{\mathrm{I}} h}{k_{\mathrm{F}} w_{\mathrm{F}} s}\left[\ln\left(\frac{h}{2 r_{\mathrm{w}}}\right) - \frac{\pi}{2}\right] \tag{1}$$

where m_{wD} is the dimensionless pseudo bottom hole flowing pressure solution corresponding to the constant flow rate; ~ represents in Laplace space; k_{I} is the permeability of inter-fracture flow zone, mD; x_{F} is the half length of the main fracture, m; k_{F} is the permeability of the main fracture flow zone, mD; w_{F} is the width of the main fracture, m; s is the Laplace transform parameter; r_{w} is the wellbore radius, m; α_{F} is the hydraulic fracture parameter in the trilinear flow model.

The hydraulic fracture parameter is defined as Eq. (2):

$$\alpha_{\mathrm{F}} = \frac{s}{\eta_{\mathrm{FD}}} + \frac{2}{C_{\mathrm{FD}}}\left(\sqrt{\frac{\beta_{\mathrm{O}}}{y_{\mathrm{eD}} C_{\mathrm{RD}}} + s} \cdot \tanh\left[\sqrt{\frac{\beta_{\mathrm{O}}}{y_{\mathrm{eD}} C_{\mathrm{RD}}} + s}\left(y_{\mathrm{eD}} - \frac{w_{\mathrm{D}}}{2}\right)\right]\right) \tag{2}$$

with

$$\beta_O = \sqrt{\frac{s}{\eta_{OD}}}\tanh\left[\sqrt{\frac{s}{\eta_{OD}}}(x_{eD}-1)\right] \tag{3}$$

where η_{FD} is the dimensionless main fracture diffusivity; η_{OD} is the dimensionless matrix flow zone diffusion coefficient; C_{RD} is the dimensionless reservoir conductivity; C_{FD} is the dimensionless fracture conductivity; y_{eD} is the dimensionless fracture spacing; w_D is the dimensionless main fracture width; x_{eD} is the dimensionless reservoir size in the x-direction.

To describe the seepage flow characteristics of shale gas reservoirs in the absence of inter-well interference, a trilinear seepage model with an infinite outer boundary condition in the reservoir matrix flow zone is also established. The dimensionless pseudo bottom hole flowing pressure solution corresponding to the constant flow rate considering the skin effect is obtained is obtained as Eq. (4):

$$\tilde{m}_{wD} = \frac{k_l x_F}{2k_F w_F s\sqrt{s_F'}\tanh(\sqrt{s_F'})} + \frac{k_l h}{k_F w_F s}\left[\ln\left(\frac{h}{2r_w}\right)-\frac{\pi}{2}\right] \tag{4}$$

with

$$s_F = \frac{s}{\eta_{FD}} + \frac{2}{C_{FD}}\left(\sqrt{\frac{\delta_O}{y_{eD}C_{RD}}+s}\cdot\tanh\left[\sqrt{\frac{\delta_O}{y_{eD}C_{RD}}+s}\left(y_{eD}-\frac{w_D}{2}\right)\right]\right) \tag{5}$$

$$\delta_O = \sqrt{\frac{s}{\eta_{OD}}} \tag{6}$$

In order to verify the correctness of the model solution without considering the interference between wells, make x_{eD} in Eq. (3) be equal to infinity. At this time, Eq. (1) is equal to Eq. (4). Therefore, the correctness of the model solution without considering the inter-well interference can be proved.

For Eqs. (1) and (4), the dimensionless pseudo bottom hole flowing pressure solution corresponding to the constant flow rate when considering the wellbore storage effect is shown as Eq (7). The detailed derivation process, related dimensionless definitions, and the meaning of other parameters in above equations are shown in Appendix B.

$$\tilde{m}_{wD,storage} = \frac{\tilde{m}_{wD}}{1+C_D s^2 \tilde{m}_{wD}} \tag{7}$$

where C_D is the dimensionless wellbore storage coefficient.

It is worth to mention that Eq. (7) is the solution in Laplace space, so that numerical Stehfest algorithm (Stehfest, 1970) can be used to obtain dimensionless pseudo pressure solutions in real time space.

2.2. Pressure deconvolution

Shale gas production data are usually over time. However, the outer boundary condition of the seepage mathematical model is usually a constant flow rate. As a result, the production data needs to be normalized before analysis. The traditional method of normalizing the data, such as using the combination of rate normalized pressure and superposition time, can lead to data points from typical pressure curves in the normalized data being scattered and fluctuating widely due to production data noise. Consequently, the matching of the normalized data with the theoretical model will be poor, leading to uncertainties in parameter interpretation. Based on this concern, a pressure deconvolution algorithm based on B-spline with nonlinear regularization (Liu et al., 2018) is introduced.

Given the variable flow rate q and the corresponding pseudo pressure m, this technique, which is based on Duhamel's principle, can be used to calculate the pseudo pressure m_u per unit flow rate through Eq. (8).

$$m_{ini} - m = \int_0^t q(t-\tau)m_u'(\tau)\mathrm{d}\tau \tag{8}$$

The implementation process of pressure deconvolution algorithm is as follows: Firstly, the sum of weights of Ilk second-order B-spline functions is used to reconstruct the derivative of pseudo pressure m_u' per unit flow rate. Secondly, using the mathematical properties of convolution integral, the sensitivity matrix of deconvolution calculation is solved quickly by piecewise integration according to the actual flow history. Finally, the idea of curvature minimization (von Schroeter et al., 2004) is introduced for the nonlinear regularization. What's more, the pseudo pressure m_u per unit flow rate calculated from Eq. (8) is compared with the theoretical model as a direct constraint on the cardinality of B-splines and the value of smoothing factor in the nonlinear regularization process.

Using this pressure deconvolution algorithm, the raw flowing pressure production data can be converted into flowing pressure per unit flow rate so as to match the inner boundary conditions of the theoretical flow model. This approach can effectively minimize the impact of data errors, prevent data from diverging, and broaden the investigation range of interpretation for typical curve analysis. Additionally, it can also reduce the production requirements for shale gas production data analysis, which does not require long period of shut-in or even shut-in. In addition, the pressure deconvolution algorithm has the advantages of high stability and fast calculation speed, which can process huge amounts of production data quickly and accurately (Liu et al., 2018).

Although this pressure deconvolution algorithm has many advantages, studies have shown that the following two basic requirements should be met for pressure deconvolution calculation (John and Lee., 2013).

1) The interpretation model remains unchanged in the process of interpreting historical production data.
2) The pressure deconvolution algorithm can only be used in linear or linearized problems (such as linear liquid flow model, linearized gas flow model, etc.), and then Duhamel's principle can be applicable.

2.3. Dynamic production data analysis method in consideration of inter-well interference in shale gas reservoirs

For the development of infill well patterns in shale gas reservoirs, it is assumed that interference can occur only between adjacent wells due to the extremely tight shale reservoir. As a result of the inter-well interference, it is expected that outer boundary conditions similar to closed boundary conditions will develop between adjacent wells, with no fluid flow at the outer boundary. Based on this assumption, the analysis of typical curves of single well dynamic production data can be undertaken to interpret fracture and reservoir parameters and to predict recoverable reserves. Subsequently, the same typical curve analysis is carried out on the dynamic production data from adjacent wells to interpret reservoir parameters and fracture parameters and predict recoverable reserves. Then, analysis of the later morphological aspects of the log-log typical curves of pseudo pressure drop and pseudo

pressure drop derivative is carried out by fitting dynamic production data from multiple wells on the same well platform. Through this analysis, the intensity of inter-well interference can be determined for wells on the same platform. If the log-log typical curves converge faster and rise more obviously at the later stage, the intensity of inter-well interference is greater. In addition, through the time corresponding to the intersection point of the log-log typical curves of the model under the closed outer boundary condition and the log-log typical curves of the model under the infinite outer boundary condition, a more intuitive method for judging the inter-well interference intensity of horizontal wells on the same well platform is proposed. For the multi-stage fractured horizontal wells of the same well platform, the reservoir geological characteristics are generally similar. Therefore, the analysis results of inter-well interference intensity of wells on the same well platform are more convincing. Since it is not affected by interference, the later stage of the log-log typical curves made by the model under the infinite outer boundary condition continues to be a linear flow regime of reservoir matrix with a slope of 0.5. Therefore, it has an intersection with the log-log typical curves made by the model under closed outer boundary conditions. The sooner or later the intersection occurs represents the intensity of inter-well interference. The overall analysis process of inter-well interference in shale gas reservoirs by production data analysis method based on deconvolution is shown in Fig. 3. Among them, the specific process of typical curves analysis for a single well is as follows.

Production data for shale gas in engineering are usually nonlinear pressure data at variable flow rate. However, the solution of the mathematical model for multi-stage fractured horizontal wells in shale gas reservoirs in Section 2.1 is the pseudo pressure corresponding to constant flow rate. Therefore, before analyzing the dynamic production data, the pressure data should be converted to pseudo pressure, so as to linearize the pressure data firstly. Then, the pseudo pressure data corresponding to variable flow rate q is transformed into the pseudo pressure m_u corresponding to constant flow rate by using the deconvolution algorithm based on Duhamel's principle in Section 2.2, so as to realize the normalization of production data. At the same time, regulation parameters including B-spline base and smoothing factor are adjusted to reduce the noise of the oscillating production data during deconvolution calculation. Finally, the log-log typical curves of pressure production data with respect to pseudo pressure & pseudo pressure derivative are analyzed by using the established mathematical model solution of multi-stage fractured horizontal wells. In particular, known fracturing data such as number of clusters, horizontal well length, reservoir thickness, wellbore radius, etc. can be used as constraints of parameter adjustment of mathematical solution to fit the actual pressure production data. Then, fracture conductivity, fracture half-length, flow regimes and reservoir parameters such as outer boundary distance, permeability, porosity and so on are also interpreted. What's more, by means of Duhamel's principle, the flow rate solution per unit pseudo pressure drop is calculated by convolution, and then the flow rate solution corresponding to variable pseudo pressure (drop) can be obtained. According to the interpreted fracture parameters and reservoir parameters, combined with the flow rate solution corresponding to variable pseudo pressure, the gas recoverable reserves of multi-stage fractured horizontal wells in shale gas reservoirs can be predicted.

The pressure deconvolution algorithm used in the dynamic production data analysis method in this paper adopts analytical method, which is more than 20 times faster than that of von Schroeter algorithm (von Schroeter et al., 2004) applied by KAPPA software (Liu et al., 2018). Therefore, deconvolution calculation of a large amount of pressure data can be done quickly. Nonlinear regularization is also used to enhance the stability of the algorithm. At the same time, appropriate constraint condition of deconvolution calculation parameter regulation (Liu et al., 2018) is added to

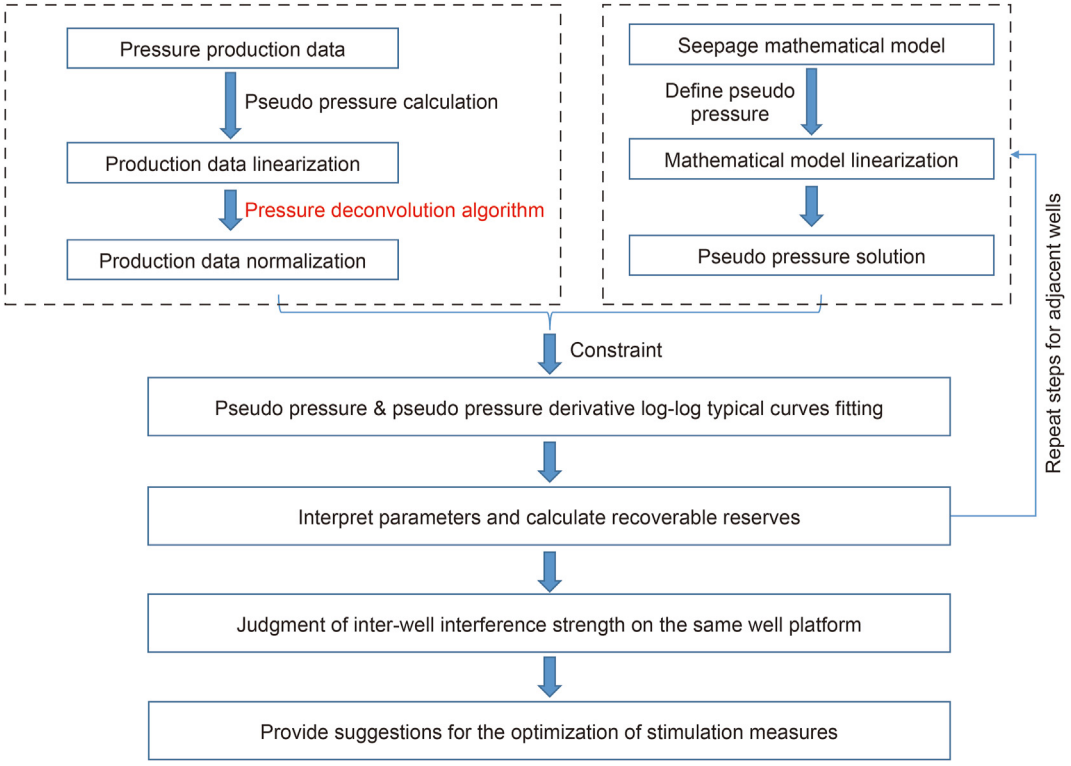

Fig. 3. Analysis process of inter-well interference in shale gas reservoirs by production data analysis method based on deconvolution.

avoid the excessive smoothing of typical curves. Different from traditional typical curves analysis method, this dynamic production data analysis method combines deconvolution calculation with typical curves fitting. By using the constraint conditions of adjusting B-spline cardinality and smoothing factor proposed in the nonlinear regularization process of pressure deconvolution (Liu et al., 2018), the normalized parameter debugging of pressure deconvolution calculation and the parameter debugging of seepage theory model calculation are mutually restricted in the process of typical curves fitting (Liu, 2019). In addition, hydraulic fracturing date and static reservoir data are taken as the condition constraints. The combination of these multiple constraints significantly reduces the potential for multiple interpretation results. The application of our proposed deconvolution algorithm to the analysis of production data for inter-well interference in shale gas reservoirs overcomes the challenges posed by complex multi-well mathematical models and poor stability of multi-well deconvolution algorithms in analysis methods of traditional typical curves. This study is of considerable significance for identifying inter-well interference and interpreting parameters with greater reliability.

3. Results and discussion

3.1. Analysis of isolated single well

Simonette, as the main Devonian development block in the Western Canada Sedimentary Basin is rich in shale gas, and 108 wells have been put into production by September 2020. The main target layer is the shale of Duvernay Formation. The effective thickness of the reservoir is 30–45 m, total organic carbon content (TOC) is 2%–6%, effective porosity is 3%–6%, permeability is 0.0001–0.0006 mD, and adsorbed gas content is 0.5–2.5 m^3/t. The shale gas production rate data and pseudo bottom hole flowing pressure data from daily dynamic production monitoring are shown in Fig. 4. Those points where production rate is 0 represent shut-in operations. The cumulative shale gas production is 40.3624×10^6 m^3. And the average daily production is 14483 m^3/d. It is known that the initial pressure of gas reservoir is 62 MPa, the reservoir temperature is 115 °C, and the reservoir thickness is 41 m. The wellbore radius is 0.107 m, the horizontal length of the horizontal well is 1962 m, the number of fracture segments of hydraulic fracturing is 21. The distance from the nearest well is about 3700 m. It can be considered an isolated well.

The pseudo bottom hole flowing pressure data are processed according to the rate normalized pressure (RNP) and the combination of material balance time (MBT) method (Hasan and Mattar, 2017; Clarkson et al., 2020), and then the log-log typical curves of pseudo pressure drop and pseudo pressure drop derivative are obtained by calculation, as shown in Fig. 5. The longitudinal coordinates RNP_p/RNP_p' represent rate normalized pressure and rate normalized pressure derivative respectively. It is evident that raw data obtained from shale gas reservoirs often exhibit significant fluctuations and divergence, thereby impeding the identification of typical seepage flow regimes in shale gas reservoirs. These factors render typical curves analysis challenging, especially when attempting to fit the collected data with mathematical models.

The Duhamel's principle is applicable because the well production process has no other technical measurements, the interpretation model has not changed, and the production data have also been linearized. Therefore, the pressure deconvolution algorithm can be used to normalize the production data, and then the actual pressure and flow data directly obtained by the field project can be converted into the corresponding pseudo bottom hole flowing pressure per unit flow rate. The calculation results are shown in Fig. 6. It can be seen that despite the effects of frequent shut-in operations, the calculated pseudo pressure data per unit flow rate becomes physically smooth and natural because the deconvolution algorithm can not only normalize the oscillating production data but also eliminate the effects of data noise. Therefore, this method has significant advantages for shale gas wells with frequent shut-ins. The abscissa in Fig. 6 reflects real time, providing a more intuitive and accurate depiction of the corresponding pressure changes during the production time. Then the normalization parameter adjustment of deconvolution calculation and the parameter adjustment of theoretical seepage flow model calculation are mutually restricted in the process of typical curves fitting. Taking known parameters such as initial formation pressure, reservoir thickness, number of clusters and wellbore radius as constraints, unknown parameters such as half-length of main fracture, outer boundary distance, permeability, porosity and comprehensive compression coefficients of main fracture & interfracture flow zone & reservoir matrix flow zone are adjusted to achieve the log-log typical curves fitting and pseudo pressure drop data per unit flow rate fitting. Fig. 7(a) shows the fitting results of the log-log typical curves of the pseudo pressure drop & pseudo pressure drop derivative per unit flow rate calculated by deconvolution and the ones calculated by the seepage flow theoretical model. Fig. 7(b) shows the fitting results between the pseudo pressure drop data per unit flow rate calculated by deconvolution and the ones calculated by seepage flow theoretical model. It can be seen that the curve fitting effect is excellent due to the mutual restriction between deconvolution calculation parameter adjustment and seepage flow model calculation parameter adjustment.

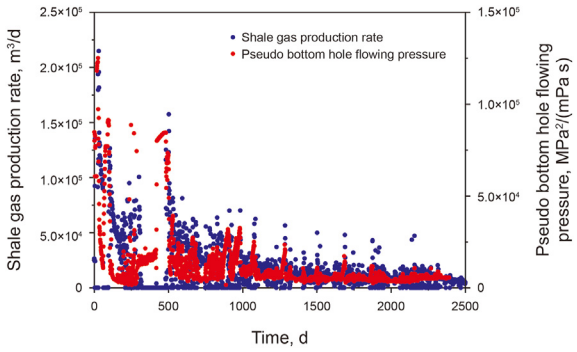

Fig. 4. Shale gas production rate and pseudo bottom hole flowing pressure of the multi-stage fractured horizontal well.

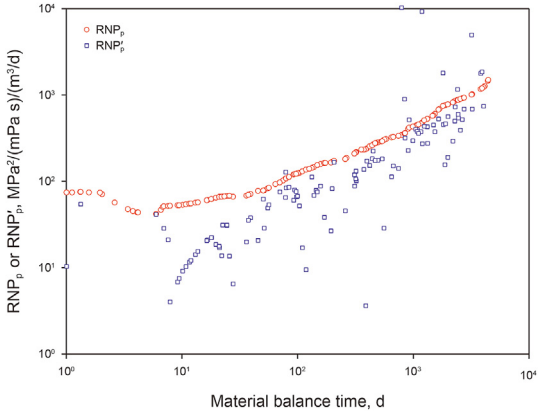

Fig. 5. The log-log typical curves of pseudo pressure drop & pseudo pressure drop derivative corresponding to RNP-MBT method.

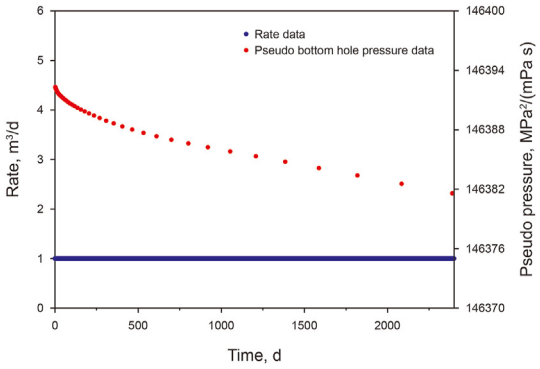

Fig. 6. Pseudo bottom hole flowing pressure data per unit flow rate.

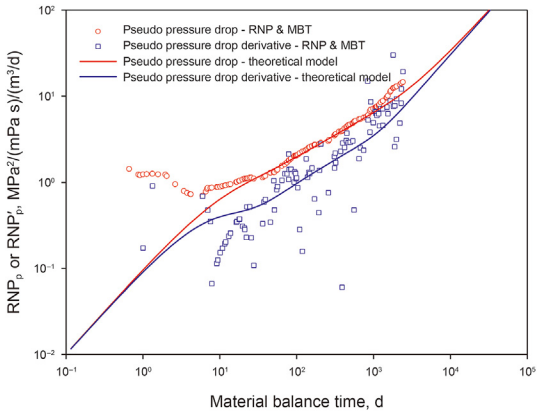

Fig. 8. Fitting results diagram of log-log typical curves of pseudo pressure drop & pseudo pressure drop derivative per unit flow rate by using RNP & MBT method.

Fig. 8 shows the fitting results of the log-log typical curves of the pseudo pressure drop and pseudo pressure drop derivative per unit flow rate calculated with RNP-MBT method, and the ones calculated by the seepage theoretical model. Obviously, compared with Fig. 7(a), the log-log typical curves of the pseudo pressure drop & pseudo pressure drop derivative per unit flow rate calculated by deconvolution fits very well with the ones calculated by the seepage theoretical model. It eliminates data errors and greatly reduces the uncertainty of interpretation results. In contrast, the log-log typical curves of the pseudo pressure drop & pseudo pressure drop derivative per unit flow rate calculated by RNP & MBT method is poorly fitted with the ones calculated by the seepage flow theoretical model. It proves the strong superiority of application of deconvolution algorithm into pressure transient analysis of production data. What's more, due to the nonlinear regularization and using B-spline function, the algorithm has good robustness. Therefore, the method incorporating deconvolution has obvious advantages in the field of typical curve analysis of a large number of dynamic shale gas production data.

The results of interpretation parameters are shown in Table 1. The bottom hole flowing pressure in the final stage of production is 9 MPa, and it is set to continue mining for 30 years with this constant pressure. Production rate prediction is carried out by using interpretation parameters and flow rate solution of seepage flow model corresponding to variable pseudo pressure. As shown in Fig. 9, although the production data are very scattered, the production rate calculated by the seepage flow model is in good agreement with the actual production rate on site. The calculated shale gas recoverable reserve of the well is also shown in Table 1.

Table 1
The results of interpretation parameters of an isolated well.

Parameter	Value
Half-length of main fracture, m	45
Potential range of the interference, m	800
Average conductivity of main fracture, mD cm	16.5
Permeability of inter-fracture flow zone, mD	0.3
Permeability of reservoir matrix flow zone, mD	0.0006
Porosity of main fracture	0.15
Porosity of inter-fracture flow zone	0.05
Porosity of reservoir matrix flow zone	0.04
Composite compressibility of main fracture, MPa^{-1}	0.004
Composite compressibility of inter-fracture flow zone, MPa^{-1}	0.0004
Composite compressibility of reservoir matrix flow zone, MPa^{-1}	0.001
Predicted shale gas recoverable reserve, m^3	5.7×10^7

By analyzing log-log typical curves of the pseudo pressure drop and pseudo pressure drop derivative in Fig. 10, five significant typical seepage flow regimes in the production process of shale gas reservoirs by a multi-stage fractured horizontal well can be identified. The five stages of the production process are defined by four black dotted lines on the graph. Starting from the leftmost side, the

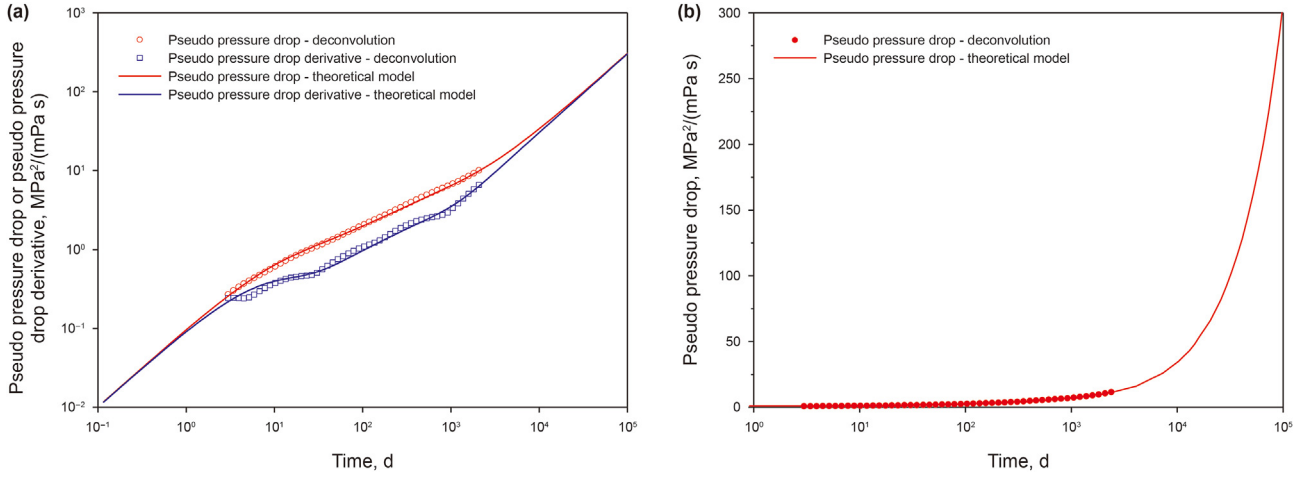

Fig. 7. Curve fitting effect diagram. (**a**) The log-log typical curves of normalized pseudo pressure drop & pseudo pressure drop derivative per unit flow rate; (**b**) Pseudo pressure drop data per unit flow rate.

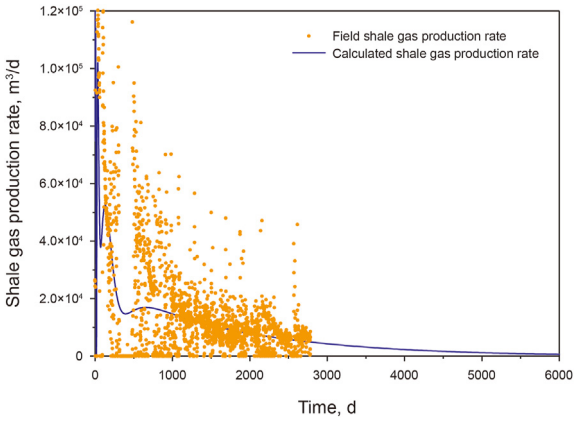

Fig. 9. Fitting result diagram of calculated shale gas production rate and field shale gas production rate data.

first stage represents the early linear flow regime of the inter-fracture flow zone. This regime is mainly shale gas flowing from the inter-fracture flow zone into the main fractures. Due to the high conductivity of the main fracture, the reservoir pressure in the inter-fracture flow zone will decrease significantly. Depending on the rapid release of elastic energy (including desorption of adsorbed gas) in the inter-fracture flow zone, shale gas is squeezed into the main fracture. The slope of the pseudo pressure and pseudo pressure derivative curve at this stage is 0.5, and the duration is short (10 d). The second is the transition flow regime 1. It is a transition from linear flow mainly in inter-fracture flow zone to linear flow mainly in reservoir matrix flow zone. The third is the medium linear flow regime in the reservoir matrix zone. The reservoir pressure drop in the inter-fracture flow zone at this regime has stabilized. Shale gas in the reservoir matrix flow zone flows gently and steadily into the inter-fracture flow zone around the horizontal well under pressure gradient. The slope of the pseudo pressure and pseudo pressure derivative curve at this stage is also 0.5, but the duration is relatively long (1000 d). That is because the single well is basically not affected by the surrounding wells, and the intensity of inter-well interference is extremely weak. The fourth is the transition flow regime 2. It is a transition from linear flow mainly in reservoir matrix flow zone to outer boundary-dominated flow. And the fifth is the outer boundary-dominated flow regime in which the later flow reaches the outer boundary. And the entire flow process at this regime begins to be dominated by the outer boundary. The pressure and pressure derivative curve slope value is 1.0 in the fifth regime. And the occurrence time of this regime (10000 d) is closely related to factors such as horizontal well spacing and outer boundary distance.

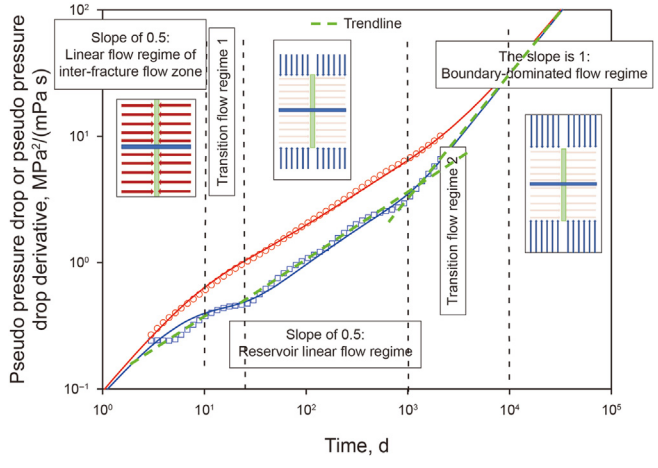

Fig. 10. Division diagram of flow regimes based on log-log typical curves of pseudo pressure drop & pseudo pressure drop derivative per unit flow rate calculated by deconvolution.

3.2. Analysis of multiwells with interference

Moreover, the typical curves of 6 multi-stage fractured horizontal wells in shale gas reservoirs with different well spacing in Duvernay area are analyzed by using the production data analysis method of shale gas reservoirs. The location of each well with different well spacing is illustrated in Fig. 11. Among them, well 1 is the isolated well analyzed in Section 3.1. Wells 2 and 3 are two wells selected from the middle of the same well platform. Wells 4, 5, and 6 are three wells selected from the middle of another well platform. The well spacing of horizontal wells in the same well platform is approximately equal, and the production pressure drop conditions of wells on the same well platform are roughly the same. The fitting results of pseudo pressure drop & pseudo pressure drop derivative log-log typical curves for the other five wells except well 1 are shown in Appendix C. It is worth noting that the pressure derivative curves of some wells show two concave shapes in the results of log-log typical curve fitting, and dual-porosity model in the analysis of typical curves may be used instead of the single-porosity one for enhancing the fitting performance due to the model extensibility in the proposed typical curve analysis method for shale gas reservoirs.

The average conductivity of main fracture, half-length of main

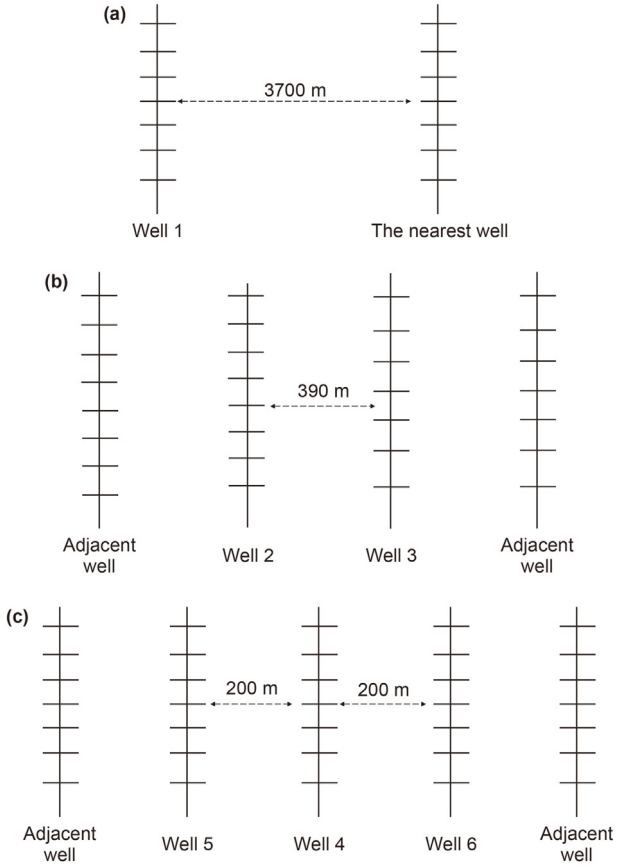

Fig. 11. Multi-stage fractured horizontal well location diagram. Location diagram of well 1 (**a**), wells 2 and 3 (**b**), and wells 4, 5, and 6 (**c**).

fracture, the distance of outer boundary, permeability of matrix, porosity of matrix, comprehensive compression coefficient of inter-fracture flow zone, comprehensive compression coefficient of reservoir matrix flow zone, and gas recoverable reserves are interpreted. It is worth to mention that for any two adjacent multi-stage fractured horizontal wells, a closed outer boundary (Ahmadi et al., 2022) effect may be generated between the wells due to inter-well interference. Results of parameter interpretation are shown in Table 2.

Table 2 reveals that the potential range formed by inter-well interference of isolated wells is the largest of all. For wells with a spacing of 390 m, the range of the potential formed by inter-well interference of well 2 is smaller than that of well 3. As a result, the predicted recoverable gas reserves of well 2 are also less than those of well 3. Furthermore, for wells with a spacing of 200 m, the range of the potential formed by inter-well interference of well 4 is smaller than that of wells 5 and 6. Similarly, the predicted recoverable gas reserves of well 4 are obviously smaller than those of wells 5 and 6. The closed outer boundary response shown in the results of the potential range of the interference interpretation in Table 2 and field data typical curve fitting in Appendix C also effectively supports the proposed conceptual model.

Fig. 12 shows the relationship between the amount of proppant per section and main fracture half-length. The graph shows that there is a positive correlation between fracture half-length and amount of proppant per section. This observation provides further affirmation of the effectiveness of the proposed method of dynamic production data analysis.

Through the analysis of the parameter interpretation results in Tables 2 and it can be seen that for the well with 3700 m far from the closest well, the interpreted potential range of the interference is much smaller than the well spacing. Consequently, it can be concluded that the reservoir is not being utilized efficiently in this particular well. For two groups of adjacent wells with well spacing of 390 and 200 m, the sum of the interpreted potential range of the interference is just approximately equal to the well spacing. Additionally, it is worth noting that as the well spacing decreases, the interpreted potential range of interference becomes shorter as well. Therefore, the inter-well interference intensity of wells with close spacing is greater than that of wells with large spacing. All areas of the reservoir between the adjacent wells can be considered effectively developed. In other words, compared with the multi-stage fractured horizontal wells with well spacing of 3700 m, the wells with well spacing of 390 and 200 m have a higher degree of reservoir utilization. The well with well spacing of 3700 m has the longest average fracture half-length and the highest average conductivity of main fracture. The average conductivity of main fracture and the average fracture half-length of the other five wells are relatively small. This corresponds with actual engineering practices, where a smaller well spacing requires a longer horizontal well length and a greater number of fracturing segments in order to lessen inter-well interference and ensure recoverable reserves. This observation is further supported by the analysis presented in Table 2. It is known that excessive fracturing scale usually causes inter-well interference to damage productivity (Ayers et al., 2018). When the adjacent horizontal wells on a well platform are fractured synchronously, the formation deformation and stress change are caused by fracturing fluid injection and rock fracturing. It will affect fracture propagation path and fracturing effect (Tang et al., 2022). With this in mind, it is recommended to use a lower average amount of proppant per stage for wells that are located in

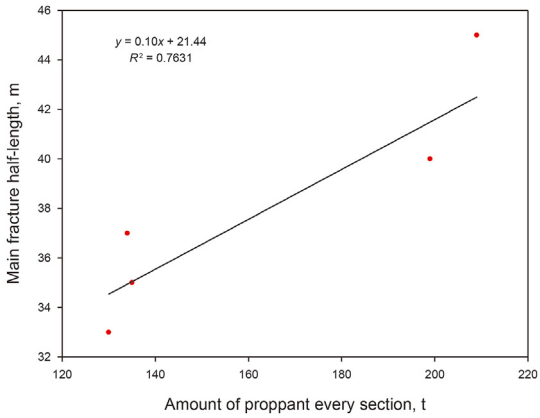

Fig. 12. Relationship between amount of proppant every section and main fracture half-length.

Table 2
The interpretation results of the parameters of wells with different spacing.

Data type	Parameter	Well number					
		Well 1	Well 2	Well 3	Well 4	Well 5	Well 6
Practical data	Well spacing, m	3700	390	390	200	200	200
	Initial reservoir pressure, MPa	62	59	60	59.2	59.2	59.2
	Horizontal well length, m	1962	2084	2200	2861	2900	2873
	Reservoir thickness, m	41	38	36	36	36.9	36.9
	Number of fracturing segments	21	30	32	57	58	57
	Stage spacing, m	93.4	69.4	68.7	50.2	49.8	50.4
	Amount of proppant/section, t	209	199	199	135	134	130
Interpretation data	Average conductivity of main fracture, mD cm	16.5	6.0	6.3	6.3	9.0	8.1
	Main fracture half-length, m	45	40	40	35	37	33
	The potential range of the interference, m	800	380	400	180	220	220
	Matrix permeability, mD	6e-4	1e-4	1e-4	2e-4	1e-4	1.8e-4
	Matrix porosity, %	0.04	0.02	0.03	0.05	0.03	0.055
	Matrix comprehensive compressibility, MPa^{-1}	1e-3	3e-3	4e-3	2.3e-3	8e-3	5e-3
	Inter-fracture flow zone comprehensive compressibility, MPa^{-1}	4e-4	4e-3	2.5e-3	2e-3	2.5e-3	2e-3
	Predicted gas recoverable reserves, m^3	5.7e7	4.4e7	5.8e7	3.9e7	7.3e7	8.7e7

close proximity to each other. Consequently, the interpreted half length of fracture and conductivity of fracture tend to decrease, with a more noticeable reduction in half length of fracture.

Based on the analysis of wells with the same well spacing and nearly the same horizontal well length, it is found that estimated recoverable reserves are closely related to the average conductivity of main fracture and matrix porosity. Specifically, a higher average conductivity of the primary fracture and greater matrix porosity tend to result in larger recoverable gas reserves. Analysis of six wells shows that the length of horizontal wells is closely related to the predicted recoverable gas reserves. In other words, the longer the horizontal well, the greater the predicted recoverable gas reserves for the well. Additionally, it has also been noted that the comprehensive compression coefficient of the matrix is positively associated with the predicted recoverable gas reserves. What's more, the interpreted matrix comprehensive compressibility value is just in the order of 0.001 MPa^{-1}, which indicates that desorption function of shale gas is much weaker than that of coalbed methane.

Fig. 13 shows the comparison of log-log typical curves of the normalized pseudo pressure actual data corresponding to unit flow rate of 6 wells calculated by the pressure deconvolution algorithm. They are divided into three groups based on well spacing. This figure reflects the variation of pseudo pressure drop and pressure derivative per well corresponding to unit flow rate. It is evident that for the isolated well, the linear flow regime of reservoir matrix in the middle period lasts for a long time. Since it is not disturbed by the surrounding wells, the log-log typical curves rise and converge very late in the later period. For wells 2 and 3 with a spacing of 390 m, the log-log typical curve of well 2 reaches the outer boundary-dominated flow regime with slope 1 earlier. This indicates that well 2 is more strongly interfered by adjacent wells. For wells 4, 5, and 6 with a well spacing of 200 m, compared with the other two wells, well 4 obviously reaches the outer boundary-dominated flow regime, then well 5, and finally well 6. This means that well 4 of the three wells is most affected by the adjacent well interference. Productivity index refers to daily gas production of gas wells under unit production pressure drop (Al-Rbeawi and Artun, 2019). Therefore, reciprocal of pseudo pressure drops for each well in Fig. 12 can reflect the transient change of productivity index. Then it can be inferred that the smaller the well spacing, the lower the pressure drop but the higher the productivity index, except for well 4. This is because well 4 is significantly impacted by inter-well interference. These findings align with the interpretation outcomes listed in Table 2. Specifically, because the influence of inter-well interference intensity on well 2 is stronger than that on well 3, the predicted gas recoverable reserves of well 2 are less than those of well 3. Similarly, the predicted gas recoverable reserves of well 4 are significantly less than those of wells 5 and 6 which are less affected by inter-well interference.

Table 3 shows the duration of flow regime sequence or the occurrence time of the flow regime sequence for six wells according to the characteristics of log-log typical curves. Upon comparing the duration or the occurrence time of different flow regimes, it becomes evident that the latest flow regime sequence is boundary-dominated flow regime. Moreover, it can further be observed that the linear flow regime in the reservoir matrix zone of well 1, which has the largest well spacing among the tested wells, typically lasts longer than the other wells. Additionally, the occurrence time of the outer boundary-dominated flow regime in well 1 is generally later than that observed in the other wells. It should be noted that the occurrence time of outer boundary-dominated flow regime is closely related to factors such as horizontal well spacing and outer boundary distance. In general, a larger well spacing leads to a later occurrence time for the boundary-dominated flow regime. However, due to the serious influence of inter-well interference, well 4 has the least potential. Besides, the duration of each typical flow regime in well 4 with a well spacing of 200 m is the shortest and the occurrence time of outer boundary-dominated flow regime is the earliest.

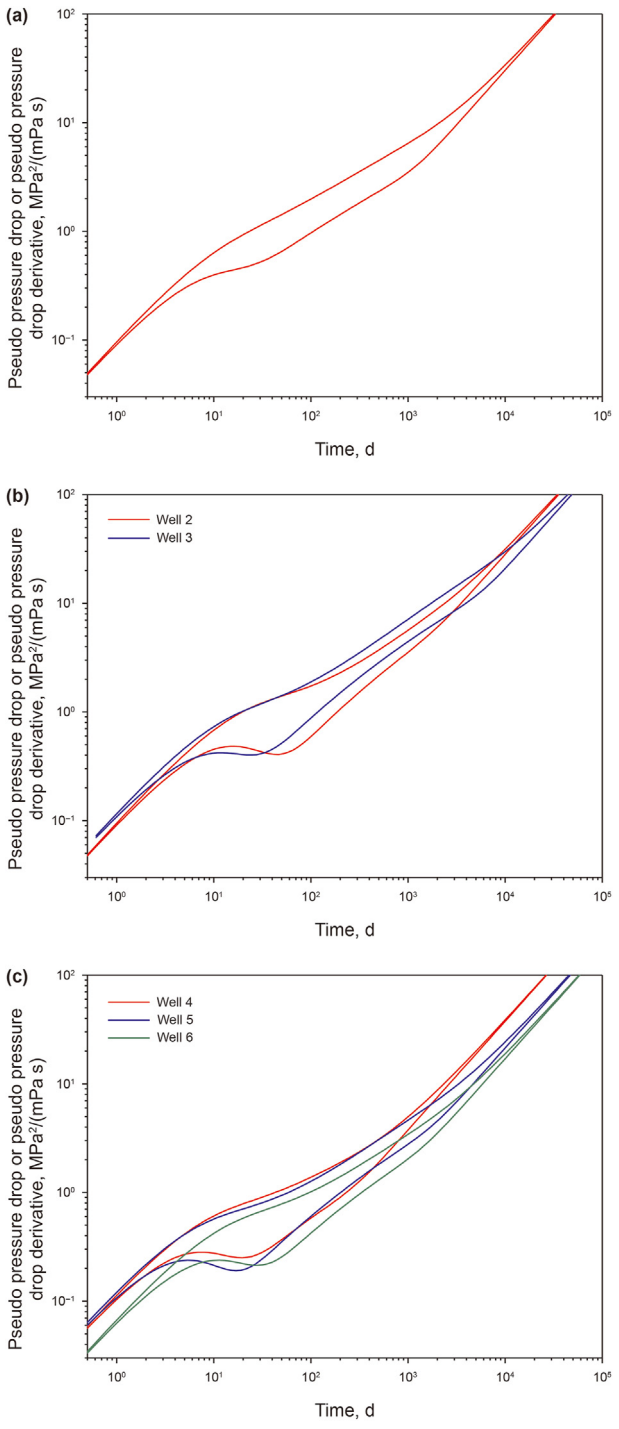

Fig. 13. Comparison chart of normalized pseudo-pressure actual data log-log typical curves of multiple wells: (**a**) Isolated well; (**b**) Wells with spacing of 390 m; (**c**) Wells with spacing of 200 m.

Table 3
Duration of flow regime sequences for six wells.

Well number	Well spacing, m	Duration of inter-fracture zone linear flow regime, d	Duration of reservoir matrix zone linear flow regime, d	Occurrence time of outer boundary-dominated flow regime, d
Well 1	3700	10	1000	10000
Well 2	390	14	200	5000
Well 3	390	32	370	13000
Well 4	200	12	56	1400
Well 5	200	13	800	5800
Well 6	200	20	700	7000

3.3. Multi-well interference judgment of the same well platform

The log-log typical curves in Fig. 13 can be used to simply compare the strength of inter-well interference effect for wells located on the same well platform. In order to further characterize the influence strength of inter-well interference more vividly, the log-log typical curves of the model under the closed outer boundary condition considering inter-well interference and the log-log typical curves of the model under the infinite outer boundary condition without considering inter-well interference are drawn. Taking wells 2 and 3 on the same well platform as an example, using the parameter results explained in Section 3.2 and the model solutions with and without inter-well interference in Section 2.1, the log-log typical curves of the model under different outer boundary conditions are shown in Fig. 14. Point A_2 is the intersection of the log-log typical curves with and without inter-well interference of well 2. And point A_3 is the intersection of the log-log typical curves with and without inter-well interference of well 3. The time corresponding to points A_2 and A_3 in the figure represents the beginning of the interference between wells. It can be observed that the time corresponding to point A_2 is approximately 2000 d, while the time corresponding to point A_3 is roughly 3200 d. The time corresponding to point A_2 is obviously earlier than that corresponding to point A_3. This indicates that the inter-well interference of well 2 is significantly stronger than that of well 3. This is consistent with the conclusion that well 2 is subject to greater inter-well interference intensity as the log-log typical curves of well 2 in Fig. 13(b) converge earlier to reach the boundary dominated flow.

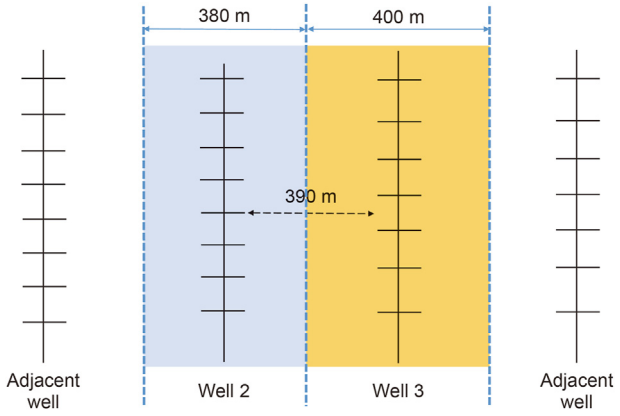

Fig. 15. The schematic diagram of the potential range formed by the interference between well 2 and well 3.

The schematic diagram of the potential range formed by the interference between well 2 and well 3 is shown in Fig. 15. The potential range of well 2 is smaller than that of well 3. This is consistent with the interpretation results obtained according to Fig. 14. Well 2 receives stronger inter-well interference. Therefore, in the case of similar reservoir conditions and production conditions, the estimated recoverable reserves of well 2 are relatively lower.

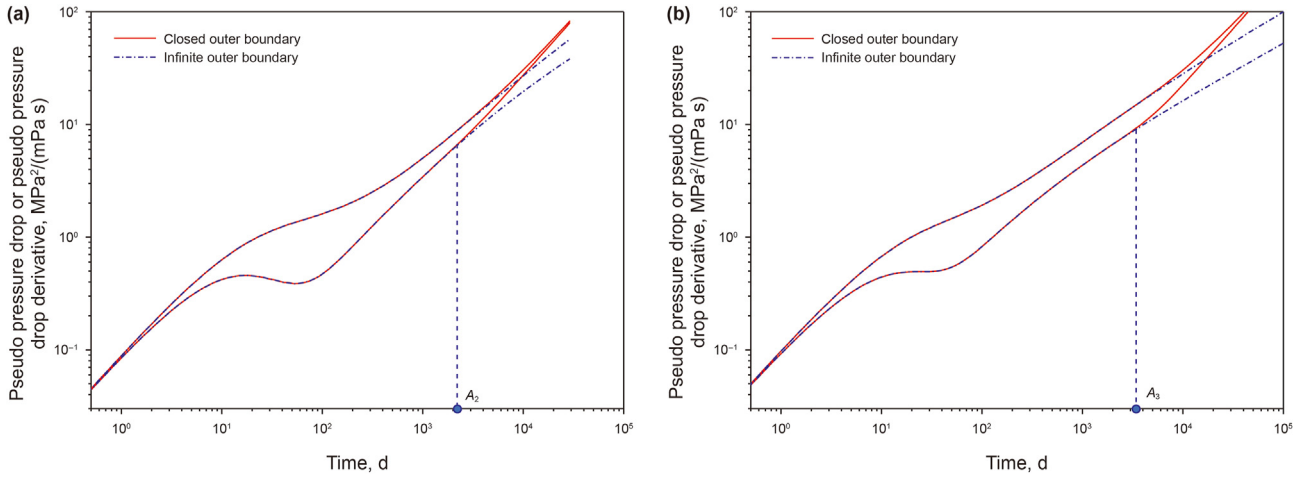

Fig. 14. The log-log typical curves of models with different outer boundary conditions. (**a**) Well 2; (**b**) Well 3.

The analysis of wells 2 and 3 from the same well platform indicates that the time sequence of the intersection point of the log-log typical curves made by the mathematical model solution of the infinite outer boundary condition and the log-log typical curves made by the mathematical model solution of the closed outer boundary condition provides a more intuitive measure of the interference strength between multiple wells. It can be helpful in optimizing mining measures to reduce inter-well interference and improve productivity.

4. Conclusions

In this paper, a novel and robust production data analysis method for studying inter-well interference in shale gas reservoirs based on pressure deconvolution algorithm was proposed. The improved pressure deconvolution algorithm is used to normalize the large-scale fluctuant dynamic production data of multi-stage fractured horizontal wells in shale gas reservoirs. By fitting log-log typical curves of the normalized dynamic production data and the pseudo pressure solutions of the established multi-well conceptual model, the production data of six actual production wells with different well spacing in Duvernay shale in West Canada Basin of North America were analyzed. Some shale reservoir parameters and fracturing characteristic parameters were interpreted. Moreover, we proposed a method for judging the strength of inter-well interference for multi-stage fractured horizontal wells located on the same well platform based on the fitted log-log typical curves. The effectiveness of the proposed method was verified through field applications. The following conclusions are drawn.

(1) The analysis method of typical curves based on deconvolution proposed in this paper can effectively solve the problem of serious fluctuation and large error of dynamic production data of a shale gas reservoir. The problem of mismatch between dynamic production data and outer boundary conditions of seepage flow model is solved. Furthermore, because the adjustment of normalization parameters of deconvolution calculation and the adjustment of model parameters of mathematical model are mutually restricted in the process of fitting typical curves, it greatly improves the fitting effect of the typical curves and reduces the multiplicity of the interpretation results.
(2) According to the slope characteristics of log-log typical curves of pseudo pressure drop and pseudo pressure drop derivative per unit flow rate fitted by this method, the flow regimes in shale gas reservoirs can be divided.
(3) The new method can reasonably interpret shale reservoir and fracture parameters such as parameters such as half length of main fracture, fracture conductivity, the potential range of inter-well interference, porosity, and comprehensive compression coefficient. As a result, the effect of fracture fracturing can be evaluated.
(4) This method can predict the recoverable reserves of multi-stage fractured horizontal wells. At the same time, it can be normalized to evaluate the productivity of different wells.
(5) For wells on the same well platform, the convergence speed of the log-log typical curves in the later period can be used to judge the strength of the inter-well interference. And the time corresponding to the intersection point of the log-log typical curves under closed outer boundary condition and infinite outer boundary condition can be used to judge the strength of inter-well interference more intuitively. The time corresponding to the intersection of the typical curves of well 2 is 2000 d, and the time corresponding to the intersection of the typical curves of well 3 is 3200 d. It indicates that the inter-well interference in well 2 is stronger than that in well 3.

The dynamic production data analysis method based on pressure deconvolution algorithm in this paper can provide technical support for the implementation of the hydraulic fracturing measurements (such as well spacing setting and fracturing spacing design) and production decline prediction in shale gas reservoirs. It is of great significance to the economic exploitation of shale gas reservoirs. However, the relevant model does not consider some complex influencing factors of seepage law in the process of shale gas reservoir exploitation such as multi-phase flow, phase behavior and so on. Therefore, in the next step, we will comprehensively consider various factors and establish an analysis method for dynamic multi-phase production data of shale gas reservoirs.

CRediT authorship contribution statement

Wen-Chao Liu: Writing – review & editing, Supervision, Software, Methodology, Investigation, Funding acquisition, Formal analysis, Conceptualization. **Cheng-Cheng Qiao:** Writing – original draft, Validation, Investigation, Formal analysis. **Ping Wang:** Project administration, Investigation, Data curation. **Wen-Song Huang:** Resources, Project administration, Data curation. **Xiang-Wen Kong:** Resources, Project administration, Investigation. **Yu-Ping Sun:** Project administration, Investigation. **He-Dong Sun:** Methodology. **Yue-Peng Jia:** Project administration, Investigation.

Declaration of competing interest

The authors declare that they have no known competing financial interests or personal relationships that could have appeared to influence the work reported in this paper.

Acknowledgement

The authors acknowledge financial support from PetroChina Innovation Foundation.

Appendix A

For any two adjacent multi-stage fractured horizontal wells on the same platform, it can be considered approximatively that the two wells are two point sources respectively; and 1D parallel flow happens between them. As shown in Fig. A.1, points M and N represent two wells respectively, and point x_T represents the location of the closed outer boundary under the influence of inter-well interference. The distance between the two point sources is the well distance, which is represented by L.

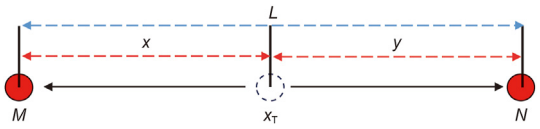

Fig. A.1. Schematic diagram of two adjacent horizontal wells in point source form.

The one-dimensional flow control equation at the point source M is established as

$$\frac{\partial^2 m}{\partial x^2}=\frac{1}{\eta}\frac{\partial m}{\partial t} \tag{A.1}$$

with

$$\eta=\frac{k}{\phi\mu C_t} \tag{A.2}$$

Shale reservoirs are extremely tight, so early rapid pressure drops occur mainly around hydraulic fractures. The later production pseudo wellbore pressure of multi-stage fractured horizontal wells is basically maintained at a constant value such as shown in Fig. 4. Define the variable $\Delta m = m_i - m(x,t)$, then the governing equations, initial conditions and boundary conditions of point source M can be written as

$$\frac{\partial^2 \Delta m_M(x,t)}{\partial x^2}=\frac{1}{\eta}\frac{\partial \Delta m_M(x,t)}{\partial t} \tag{A.3}$$

$$\Delta m_M(x,t)|_{t=0}=0 \tag{A.4}$$

$$\Delta m_M(x,t)|_{x=0}=m_\omega \tag{A.5}$$

$$\Delta m_M(x,t)|_{x\to\infty}=0 \tag{A.6}$$

where m_ω is the initial reservoir pseudo pressure minus the fixed pseudo wellbore pressure at the later stage of production. It is a fixed value.

Laplace transformation is performed on the model established above:

$$\frac{\partial^2 \mathscr{L}\{\Delta m_M(x,t)\}}{\partial x^2}=\frac{1}{\eta}\cdot s\cdot \mathscr{L}\{\Delta m_M(x,t)\} \tag{A.7}$$

$$\mathscr{L}\{\Delta m_M(x,t)\}|_{x=0}=\frac{m_\omega}{s} \tag{A.8}$$

$$\mathscr{L}\{\Delta m_M(x,t)\}|_{x\to\infty}=0 \tag{A.9}$$

The pressure solution of the model is obtained by using the general solution of the partial differential equation and the boundary conditions. The pressure distribution of the point source M is

$$\mathscr{L}\{\Delta m_M(x,t)\}=\frac{m_\omega}{s}\cdot e^{-\sqrt{\frac{s}{\eta}}\cdot x} \tag{A.10}$$

For point source N, the seepage flow model is similar to that of point source M. The difference lies in the inner boundary conditions. As adjacent wells on the same well platform, two wells have similar pressure conditions. There is a multiple relationship between the inner boundary pressure conditions of the two point sources. Therefore, its inner boundary condition is set as

$$m_N(x,t)|_{x=0}=C_0 m_\omega \tag{A.11}$$

where C_0 is a constant.

It can be obtained that the pressure distribution of point source N is

$$\mathscr{L}\{\Delta m_N(y,t)\}=C_0 m_\omega\cdot e^{-\sqrt{\frac{s}{\eta}}\cdot y} \tag{A.12}$$

By Laplace transformation correspondence, the forms of Eqs. (A.10) and (A.12) in the real space domain can be obtained as

$$\Delta m_M(x,t)=m_\omega\cdot\left(1-\frac{2}{\sqrt{\pi}}\int_0^{\frac{x}{2\sqrt{\eta t}}}e^{-x^2}dx\right) \tag{A.13}$$

$$\Delta m_N(y,t)=C_0 m_\omega\cdot\left(1-\frac{2}{\sqrt{\pi}}\int_0^{\frac{y}{2\sqrt{\eta t}}}e^{-y^2}dy\right) \tag{A.14}$$

Therefore, the flow rate at the closed outer boundary satisfies the superposition principle and can be expressed as

$$\frac{\partial \Delta m_M}{\partial x}-\frac{\partial \Delta m_N}{\partial y}=-m_\omega\cdot\frac{1}{\sqrt{\pi\eta t}}e^{-\frac{x^2}{4\eta t}}+C_0 m_\omega\cdot\frac{1}{\sqrt{\pi\eta t}}e^{-\frac{y^2}{4\eta t}}=0 \tag{A.15}$$

Eq. (A.15) can be simplified to

$$e^{\frac{x^2-y^2}{4\eta t}}=\frac{1}{C_0}=e^{C_1} \tag{A.16}$$

with

$$C_1=-\ln C_0,\quad L=x+y \tag{A.17}$$

Therefore, we can find that the distance x between the closed outer boundary and the left point source M is

$$x=\frac{4\eta t C_1}{2L}+\frac{L}{2} \tag{A.18}$$

It changes over time. However, through the calculation data of pseudo pressure drop of adjacent wells in Duvernay block, it is found that the pseudo pressure drop multiple C_0 of the two wells is usually between 0.94 and 1.06, so the constant C_1 is between −0.0583 and 0.0618. According to the reservoir parameters of the above field blocks, the calculated value of η is usually between 5.0 and 6.0 m^2/d. Therefore, when 30 years is the abandonment time of horizontal well production, the variation range of x with time is about 12.8–19.0 m.

In summary, the multi-well conceptual model with fixed closed outer boundary can be used to describe the phenomenon of multi-well inter-well interference. Although the outer boundary is indeed mobile, the range of movement is very limited. Within this limited range of variation, the idea of average is introduced. The closed outer boundary x_T is actually an average index that can quantitatively characterize the inter-well interference. In practical

applications, although factors such as formation heterogeneity, multi-well superposition and so on may also have an impact on x_T, the conceptual model still works as shown in practical application part.

Appendix B

For reservoir matrix flow zone, the equation of motion is

$$\vec{v}_O = -\frac{k_O}{\mu}\mathrm{grad}(P_O) \tag{B.1}$$

The state equation is

$$\rho_O = \frac{P_O M}{ZRT} \tag{B.2}$$

The fluid mass conservation equation is

$$\frac{\partial(\rho_O \phi_O + \rho_{sc} V_E)}{\partial t} + \mathrm{div}\left(\rho_O \vec{v}_O\right) = 0 \tag{B.3}$$

where the subscript 'O' represents the reservoir matrix flow zone; k is the permeability, mD; μ is the viscosity of shale gas, mPa s; P is pressure, MPa; Z is the gas deviation factor, dimensionless; ρ is the density of gas, kg/m^3; M is the molar mass of gas, kg/mol; R is the gas constant, 8.314 J/(mol K); ρ_{sc} is the density of gas under standard conditions, kg/m^3; V_E is the adsorption capacity of shale gas, expressed by Langmuir adsorption model, m^3/m^3.

Substitute the equation of motion and the equation of state into the conservation of mass equation and simplify

$$\frac{\partial}{\partial x}\left(\frac{P_O}{Z}\frac{\partial P_O}{\partial x}\right) = \frac{1}{\eta_O}\frac{P_O}{Z}\frac{\partial P_O}{\partial t} \tag{B.4}$$

where η_O is the diffusion coefficient in the matrix flow zone, m^2/s, and defined as follows:

$$\eta_O = \frac{k_O}{\phi_O C_{tO} \mu} \tag{B.5}$$

where C_{to} is the comprehensive compression coefficients of reservoir matrix flow zone, MPa^{-1}.

The established model is linearized by defining pseudo pressure, where the pseudo pressure is defined as Eq. (B.6):

$$m = 2\int_0^p \frac{P}{\mu Z}\mathrm{d}P \tag{B.6}$$

The model is linearized by pseudo-pressure, and then the dimensionless model is obtained

$$\frac{\partial^2 m_{OD}}{\partial x_D^2} = \frac{1}{\eta_{OD}}\frac{\partial m_{OD}}{\partial t_D} \tag{B.7}$$

The infinite outer boundary condition and internal boundary condition are shown in Eqs. (B.8) and (B.9) respectively:

$$m_{OD}|_{x=+\infty} = 0 \tag{B.8}$$

$$m_{OD}|_{x_D=1} = m_{ID}|_{x_D=1} \tag{B.9}$$

The general solution of the model is obtained by Laplace transform:

$$\tilde{m}_{OD} = A_O e^{-\sqrt{\frac{s}{\eta_{OD}}}x_D} + B_O e^{\sqrt{\frac{s}{\eta_{OD}}}x_D} \tag{B.10}$$

According to the boundary conditions, we can get

$$A_O = \frac{\tilde{m}_{ID}|_{x_D=1}}{e^{-\sqrt{\frac{s}{\eta_{OD}}}}} \tag{B.11}$$

$$\begin{aligned}\left.\frac{\partial \tilde{m}_{OD}}{\partial x_D}\right|_{x_D=1} &= -\sqrt{\frac{s}{\eta_{OD}}}\,\frac{\left.\tilde{m}_{ID}\right|_{x_D=1}}{e^{-\sqrt{\frac{s}{\eta_{OD}}}}}\cdot e^{-\sqrt{\frac{s}{\eta_{OD}}}} = -\sqrt{\frac{s}{\eta_{OD}}}\cdot\left.\tilde{m}_{ID}\right|_{x_D=1} \\ &= -\delta_O\cdot\left.\tilde{m}_{ID}\right|_{x_D=1}\end{aligned} \tag{B.12}$$

with

$$\delta_O = \sqrt{\frac{s}{\eta_{OD}}} \tag{B.13}$$

For inter-fracture flow zone, it can be similarly obtained

$$\frac{\partial^2 m_{ID}}{\partial {y_D}^2} + \frac{1}{y_{eD} C_{RD}}\left.\frac{\partial m_{OD}}{\partial x_D}\right|_{x_D=1} = \frac{\partial m_{ID}}{\partial t_D} \tag{B.14}$$

The outer boundary condition and internal boundary condition are

$$\left.\frac{\partial m_{ID}}{\partial y_D}\right|_{y_D=y_{eD}} = 0 \tag{B.15}$$

$$m_{ID}|_{y_D=\frac{w_D}{2}} = m_{FD}|_{y_D=\frac{w_D}{2}} \tag{B.16}$$

The general solution of the model is obtained by Laplace transform:

$$\tilde{m}_{ID} = A_I \exp\left(-\sqrt{S_I'}\,y_D\right) + B_I \exp\left(\sqrt{S_I'}\,y_D\right) \tag{B.17}$$

$$\frac{\partial \tilde{m}_{ID}}{\partial y_D} = -\sqrt{S_I'}A_I \exp\left(-\sqrt{S_I'}\,y_D\right) + \sqrt{S_I'}B_I \exp\left(\sqrt{S_I'}\,y_D\right) \tag{B.18}$$

with

$$S_I' = \sqrt{\frac{\delta_O}{y_{eD} C_{RD}} + s} \tag{B.19}$$

According to the boundary conditions, we can get

$$\left.\frac{\partial \tilde{m}_{ID}}{\partial y_D}\right|_{y_D=\frac{w_D}{2}} = -\beta_I' \tilde{m}_{FD}|_{y_D=\frac{w_D}{2}} \tag{B.20}$$

with

$$\beta_{\mathrm{I}}' = \sqrt{S_{\mathrm{I}}'}\tanh\left[\sqrt{S_{\mathrm{I}}'}\left(y_{\mathrm{eD}} - \frac{w_{\mathrm{D}}}{2}\right)\right] \tag{B.21}$$

For main fracture flow zone

$$\frac{\partial^2 m_{\mathrm{FD}}}{\partial x_{\mathrm{D}}{}^2} + \frac{2}{C_{\mathrm{FD}}}\frac{\partial m_{\mathrm{ID}}}{\partial y_{\mathrm{D}}}\bigg|_{y_{\mathrm{D}}=\frac{w_{\mathrm{D}}}{2}} = \frac{\partial m_{\mathrm{FD}}}{\partial t_{\mathrm{D}}} \tag{B.22}$$

$$\frac{\partial m_{\mathrm{FD}}}{\partial x_{\mathrm{D}}}|_{x_{\mathrm{D}}=1} = 0 \tag{B.23}$$

$$\frac{\partial m_{\mathrm{FD}}}{\partial x_{\mathrm{D}}}|_{x_{\mathrm{D}}=0} = -\frac{1}{2C_{\mathrm{FD}}} \tag{B.24}$$

The general solution of the model is obtained by Laplace transform:

$$\tilde{m}_{\mathrm{FD}} = A_{\mathrm{F}}\exp\left(-\sqrt{S_{\mathrm{F}}'}x_{\mathrm{D}}\right) + B_{\mathrm{F}}\exp\left(\sqrt{S_{\mathrm{F}}'}x_{\mathrm{D}}\right) \tag{B.25}$$

$$\frac{\partial \tilde{m}_{\mathrm{FD}}}{\partial x_{\mathrm{D}}} = -\sqrt{S_{\mathrm{F}}'}A_{\mathrm{F}}\exp\left(-\sqrt{S_{\mathrm{F}}'}x_{\mathrm{D}}\right) + \sqrt{S_{\mathrm{F}}'}B_{\mathrm{F}}\exp\left(\sqrt{S_{\mathrm{F}}'}x_{\mathrm{D}}\right) \tag{B.26}$$

with

$$S_{\mathrm{F}}' = \frac{s}{\eta_{\mathrm{FD}}} + \frac{2\beta_{\mathrm{I}}'}{C_{\mathrm{FD}}} \tag{B.27}$$

According to the boundary conditions, the dimensionless pseudo bottom hole flowing pressure solution corresponding to the constant flow rate considering the skin effect is obtained

$$\tilde{m}_{\mathrm{wD}} = \frac{k_{\mathrm{I}}x_{\mathrm{F}}}{2k_{\mathrm{F}}w_{\mathrm{F}}s\sqrt{S_{\mathrm{F}}'}\tanh\left(\sqrt{S_{\mathrm{F}}'}\right)} + \frac{k_{\mathrm{I}}h}{k_{\mathrm{F}}w_{\mathrm{F}}s}\left[\ln\left(\frac{h}{2r_{\mathrm{w}}}\right) - \frac{\pi}{2}\right] \tag{B.28}$$

where m_{OD}, m_{ID}, and m_{FD} are the dimensionless pseudo pressure corresponding to the pressure in reservoir matrix flow zone, inter-fracture flow zone, and main fracture zone; x_{eD} is the dimensionless closed outer boundary distance formed by inter-well interference; y_{eD} is the dimensionless half of the distance between adjacent main fractures.

Considering the wellbore storage effect, the dimensionless pseudo bottom hole flowing pressure solution corresponding to the constant flow rate is

$$\tilde{m}_{\mathrm{wD,storage}} = \frac{\tilde{m}_{\mathrm{wD}}}{1 + C_{\mathrm{D}}s^2\tilde{m}_{\mathrm{wD}}} \tag{B.29}$$

The definition of dimensionless variables in mentioned mathematical models are defined as follows:

$$m_{\mathrm{wD}} = \frac{k_{\mathrm{I}}hT_{\mathrm{SC}}}{0.0864q_{\mathrm{F}}P_{\mathrm{SC}}T}(m_{\mathrm{i}} - m_{\mathrm{F}}) \tag{B.30}$$

$$C_{\mathrm{FD}} = \frac{k_{\mathrm{F}}w_{\mathrm{F}}}{k_{\mathrm{I}}x_{\mathrm{F}}} \tag{B.31}$$

$$C_{\mathrm{RD}} = \frac{k_{\mathrm{I}}x_{\mathrm{F}}}{k_{\mathrm{O}}y_{\mathrm{e}}} \tag{B.32}$$

$$\eta_{\mathrm{FD}} = \frac{\eta_{\mathrm{F}}}{\eta_{\mathrm{I}}} = \frac{k_{\mathrm{F}}(\phi C_{\mathrm{t}})_{\mathrm{I}}}{k_{\mathrm{I}}(\phi C_{\mathrm{t}})_{\mathrm{F}}} \tag{B.33}$$

$$\eta_{\mathrm{OD}} = \frac{\eta_{\mathrm{O}}}{\eta_{\mathrm{I}}} = \frac{k_{\mathrm{O}}(\phi C_{\mathrm{t}})_{\mathrm{I}}}{k_{\mathrm{I}}(\phi C_{\mathrm{t}})_{\mathrm{O}}} \tag{B.34}$$

$$x_{\mathrm{eD}} = \frac{x_{\mathrm{e}}}{x_{\mathrm{F}}} \tag{B.35}$$

$$y_{\mathrm{eD}} = \frac{y_{\mathrm{e}}}{x_{\mathrm{F}}} \tag{B.36}$$

$$w_{\mathrm{D}} = \frac{w_{\mathrm{F}}}{x_{\mathrm{F}}} \tag{B.37}$$

$$C_{\mathrm{D}} = \frac{C}{2\pi(\phi c_{\mathrm{t}})_{\mathrm{I}}hx_{\mathrm{F}}{}^2} \tag{B.38}$$

where m_{i} is the pseudo pressure corresponding to the initial reservoir pressure calculated according to Eq. (B.6), $\mathrm{MPa}^2/(\mathrm{mPa\ s})$; k_{O} is the permeability of reservoir matrix flow zone, mD; ϕ_{O}, ϕ_{I}, and ϕ_{F} are the porosity of reservoir matrix flow zone, inter-fracture flow zone, and main fracture zone, %; η_{I} is the diffusion coefficient of inter-fracture flow zone, m^2/s; η_{F} is the hydraulic fracture diffusion coefficient, m^2/s; C_{tI} and C_{tF} are the comprehensive compression coefficients of inter-fracture flow zone and main fracture zone, MPa^{-1}; C is the wellbore storage coefficient.

The comprehensive compression coefficients of reservoir matrix flow zone and inter-fracture flow zone considering adsorption gas desorption are as follows (Wu et al., 2018):

$$C_{\mathrm{tj}} = \frac{1}{P_j} - \frac{1}{Z}\frac{\partial Z}{\partial P_j} + \frac{\rho_{\mathrm{sc}}V_{\mathrm{L}}P_{\mathrm{L}}}{\phi_j\frac{M}{RT}\frac{P_j}{Z}(P_{\mathrm{L}} + P_j)^2}, \quad (j = \mathrm{O},\ \mathrm{I}) \tag{B.39}$$

where P_j is the pressure in j zone, MPa; 'O' represents reservoir matrix flow zone and 'I' represents inter-fracture flow zone; V_{L} is the Langmuir volume, $\mathrm{m}^3/\mathrm{m}^3$; P_{L} is the Langmuir pressure, MPa; M is the molar mass of the gas, g/mol; R is the molar constant, J/(K mol).

The comprehensive compression coefficient of main fracture flow zone is shown as

$$C_{\mathrm{tF}} = \frac{1}{P_{\mathrm{F}}} - \frac{1}{Z}\frac{\partial Z}{\partial P_{\mathrm{F}}} \tag{B.40}$$

where P_{F} is the pressure in the main fracture flow zone, MPa.

Appendix C

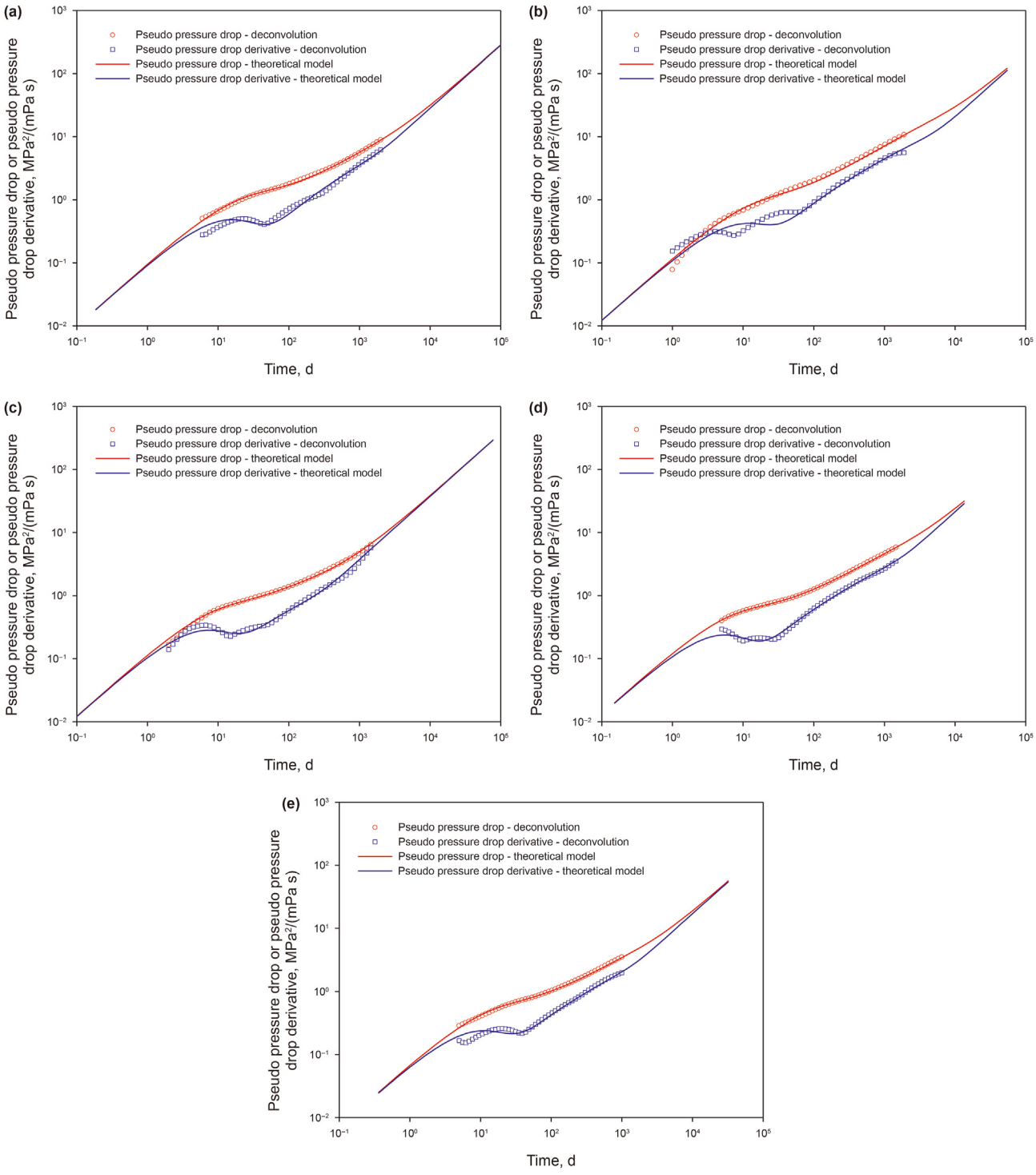

Fig. C.1. The fitting results of pseudo pressure drop & pseudo pressure drop derivative log-log typical curves for the other five wells. (**a**) Well 2; (**b**) Well 3; (**c**) Well 4; (**d**) Well 5; (**e**) Well 6.

References

Afanaskin, I.V., Kryganov, P.V., Volpin, S.G., Kolevatov, A.A., Glushakov, A.A., Yalov, P.V., 2022. Multi-well deconvolution issue solving for producing well with increasing water-cut through CRM-model application. J. Pet. Sci. Eng. 215PB, 110679. https://doi.org/10.1016/j.petrol.2022.110679.

Ahmadi, H., Hamdi, H., Clarkson, C., 2022. Rate-transient analysis for estimating the linear flow parameters of communicating wells using the dynamic drainage area (DDA) concept. J. Petrol. Sci. Eng. 218, 111038. https://doi.org/10.1016/j.petrol.2022.111038.

Alafnan, S., Awotunde, A., Glatz, G., Adjei, S., Alrumaih, I., Gowida, A., 2021. Langmuir adsorption isotherm in unconventional resources: applicability and limitations. J. Petrol. Sci. Eng. 207, 109172. https://doi.org/10.1016/j.petrol.2021.109172.

Al-Rbeawi, S., Artun, E., 2019. Fishbone type horizontal wellbore completion: a study for pressure behavior, flow regimes, and productivity index. J. Petrol. Sci. Eng. 176, 172–202. https://doi.org/10.1016/j.petrol.2018.12.076.

Al-Shami, T.M., Jufar, S.R., Kumar, S., Abdulelah, H., Abdullahi, M.B., Al-Hajri, S., Negash, B.M., 2023. A comprehensive review of interwell interference in shale reservoirs. Earth Sci. Rev. 237, 104327. https://doi.org/10.1016/j.earscirev.2023.104327.

Ayers, K., Jacot, H., Ayers, A., 2018. Statistical analysis of generational effect on marcellus well completions using bottomhole gauge data. In: SPE/AAPG Eastern Reg. Meeting. https://doi.org/10.2118/191785-18ERM-MS.

Brown, M., Ozkan, E., Raghavan, R., Kazemi, H., 2011. Practical solutions for pressure-transient responses of fractured horizontal wells in unconventional shale reservoirs. SPE Reservoir Eval. Eng. 14 (6), 663–676. https://doi.org/10.2118/125043-PA.

Chen, J.Y., Wei, Y.S., Wang, J.L., Yu, W., Qi, Y.D., Wu, J.F., Luo, W.J., 2021. Inter-well interference and well spacing optimization for shale gas reservoirs. J. Nat. Gas Geosci. 6 (5), 301–312. https://doi.org/10.1016/j.jnggs.2021.09.001.

Clarkson, C.R., Yuan, B., Zhang, Z.Z., 2020. A new straight-line analysis method for estimating fracture/reservoir properties using dynamic fluid-in-place calculations. SPE Reservoir Eval. Eng. 23 (2), 606–626. https://doi.org/10.2118/195930-PA.

Cui, Y.Z., Zhang, F.B., Jiang, R.Z., Lin, J.Q., 2022. Pressure transient behavior modeling of a multi-horizontal well pad with damaged fracture in shale gas. J. Petrol. Sci. Eng. 216, 110755. https://doi.org/10.1016/j.petrol.2022.110755.

Cumming, J.A., Wooff, D.A., Whittle, T., Gringarten, A.C., 2014. Multi-well deconvolution. SPE Reservoir Eval. Eng. 17 (4), 457–465. https://doi.org/10.2118/166458-PA.

Du, F.S., Nojabaei, B., 2020. Estimating diffusion coefficients of shale oil, gas, and condensate with nano-confinement effect. J. Petrol. Sci. Eng. 193, 107362. https://doi.org/10.1016/j.petrol.2020.107362.

Ge, X., Guo, T.L., Ma, Y.S., Wang, G.L., Li, M.W., Zhao, P.R., Yu, X.Q., Li, S.G., Fan, H.J., Zhan, T., 2022. Fracture development and inter-well interference for shale gas production from the Wufeng-Longmaxi Formation in a gentle syncline area of Weirong shale gas field, southern Sichuan, China. J. Petrol. Sci. Eng. 212, 110207. https://doi.org/10.1016/j.petrol.2022.110207.

Gupta, I., Rai, C., Sondergeld, C., Devegowda, D., 2018. Variable exponential decline: modified Arps to characterize unconventional-shale production performance. SPE Reservoir Eval. Eng. 21 (4), 1045–1057. https://doi.org/10.2118/194005-PA.

Gupta, I., Rai, C., Devegowda, D., Sondergeld, C., 2020. Haynesville shale: predicting long-term production and residual analysis to identify well interference and fracture hits. SPE Reservoir Eval. Eng. 23 (1), 132–142. https://doi.org/10.2118/195673-PA.

Hasan, S.S., Mattar, L., 2017. Does unit-slope beyond maximum producing time always represent BDF in RTA? In: SPE Unconv. Resour. Conf. https://doi.org/10.2118/185020-MS.

He, Y., He, Z., Tang, Y., Xu, Y., Long, J., Sepehrnoori, K., 2023. Shale gas production evaluation framework based on data-driven models. Petrol. Sci. 20 (3), 1659–1675. https://doi.org/10.1016/j.petsci.2022.12.003.

Ilk, D., Valko, P.P., Blasingame, T.A., 2006. Deconvolution of variable-rate reservoir-performance data using B-splines. SPE Reservoir Eval. Eng. 9 (5), 582–595. https://doi.org/10.2118/95571-PA.

Jaffrezic, V., Razminia, K., Cumming, J., Whittle, T.M., Gringarten, A.C., 2019. Application of constrained multiwell deconvolution to interfering wells in gas reservoirs with significant pressure depletion. In: SPE Ann. Tech. Conf. Exhib. https://doi.org/10.2118/195904-MS.

John, SpiveyP., Lee, John W., 2013. Applied Well Test Interpretation. Society of Petroleum Engineers, 9781613993071.

Liang, P., Aguilera, R., Mattar, L., 2017. A new method for production–data analysis and well testing by use of superposition rate. SPE Reservoir Eval. Eng. 21 (1), 1–16. https://doi.org/10.2118/185966-PA.

Liu, W.C., Liu, Y.W., Zhu, W.Y., Sun, H.D., 2018. A stability-improved efficient deconvolution algorithm based on B-splines by appending a nonlinear regularization. J. Petrol. Sci. Eng. 164, 400–416. https://doi.org/10.1016/j.petrol.2018.01.083.

Liu, W.C., 2019. Deconvolution and its Application in Production Data Analysis of Unconventional Gas Reservoirs. Science Press, Beijing, 9787030631329.

Liu, Y.Y., Ma, X.H., Zhang, X.W., Guo, W., Kang, L.X., Yu, R.Z., Sun, Y.P., 2021. A deep-learning-based prediction method of the estimated ultimate recovery (EUR) of shale gas wells. Petrol. Sci. 18 (5), 1450–1464. https://doi.org/10.1016/j.petsci.2021.08.007.

Lu, T., Li, Z.P., Lai, F.P., Meng, Y., Ma, W.L., Sun, Y.P., Wei, M.Q., 2019. Blasingame decline analysis for variable rate/variable pressure drop: a multiple fractured horizontal well case in shale gas reservoirs. J. Petrol. Sci. Eng. 178, 193–204. https://doi.org/10.1016/j.petrol.2019.03.036.

Ma, Z.W., Leung, J.Y., Zanon, S., 2018. Integration of artificial intelligence and production data analysis for shale heterogeneity characterization in steam-assisted gravity-drainage reservoirs. J. Petrol. Sci. Eng. 163, 139–155. https://doi.org/10.1016/j.petrol.2017.12.046.

Meng, J., Zhou, Y.J., Ye, T.R., Xiao, Y.T., Lu, Y.Q., Zheng, A.W., Liang, B., 2023. Hybrid data-driven framework for shale gas production performance analysis via game theory, machine learning, and optimization approaches. Petrol. Sci. 20, 277–294. https://doi.org/10.1016/j.petsci.2022.09.003.

Pan, Y., Deng, L., Lee, W.J., 2020. A novel data-driven pressure/rate deconvolution algorithm to enhance production data analysis in unconventional reservoirs. J. Petrol. Sci. Eng. 192, 107332. https://doi.org/10.1016/j.petrol.2020.107332.

Paryani, M., Smaoui, R., Poludasu, S., Attia, B., Umholtz, N., Ahmed, A., Ouenes, A., 2017. Adaptive fracturing to avoid frac hits and interference: a Wolfcamp shale case study. In: SPE Unconv. Resour. Conf. https://doi.org/10.2118/185044-MS.

Ren, W.X., Lau, H.C., 2020. New rate-transient analysis for fractured shale gas wells using a tri-linear flow model. J. Nat. Gas Sci. Eng. 80, 103368. https://doi.org/10.1016/j.jngse.2020.103368.

Sharma, P., Salman, M., Reza, Z., Kabir, C.S., 2019. Probing the roots of Arps hyperbolic relation and assessing variable-drive mechanisms for improved DCA. J. Petrol. Sci. Eng. 182, 106288. https://doi.org/10.1016/j.petrol.2019.106288.

Shi, J.T., Wu, J.Y., Sun, Z., Xiao, Z.H., Liu, C., Sepehrnoori, K., 2020. Methods for simultaneously evaluating reserve and permeability of undersaturated coalbed methane reservoirs using production data during the dewatering stage. Petrol. Sci. 17 (4), 1067–1086. https://doi.org/10.1007/s12182-019-00410-3.

Stehfest, H., 1970. Remark on algorithm 368 numerical inversion of Laplace transforms. Commun. ACM 13 (10), 624–625. https://doi.org/10.1145/361953.361969.

Tang, J., Gu, G., Liu, B., Zhang, G., Liu, Z., 2022. A laboratory-scale DEM simulation on multiwell simultaneous fracturing to improve the understanding of inter-fracture interference. J. Energy Eng. 148 (4), 04022025. https://doi.org/10.1061/(ASCE)EY.1943-7897.0000847.

Villarreal, S.Z., Moghanloo, R.G., 2022. Production data analysis for shale gas wells. Unconventional Shale Gas Development. Gulf Professional Publishing, pp. 417–432. https://doi.org/10.1016/B978-0-323-90185-7.00010-8 (Chapter 16).

von Schroeter, T., Hollaender, F., Gringarten, A.C., 2004. Deconvolution of well test data as a nonlinear total least squares problem. SPE J. 9 (4), 375–390. https://doi.org/10.2118/77688-PA.

Wang, J.L., Jia, A.L., Wei, Y.S., Qi, Y.D., Dai, Y., 2018. Laplace-domain multiwell convolution for simulating pressure interference response of multiple fractured horizontal wells by use of modified Stehfest algorithm. J. Petrol. Sci. Eng. 161, 231–247. https://doi.org/10.1016/j.petrol.2017.11.074.

Wang, K., Jiang, B.B., Li, H.T., Liu, Q., Bu, C.Z., Wang, Z.Q., Tan, Y.S., 2020. Rapid and accurate evaluation of reserves in different types of shale-gas wells: production-decline analysis. Int. J. Coal Geol. 218, 103359. https://doi.org/10.1016/j.coal.2019.103359.

Wang, Q., Jiang, F., 2019. Integrating linear and nonlinear forecasting techniques based on grey theory and artificial intelligence to forecast shale gas monthly production in Pennsylvania and Texas of the United States. Energy 178, 781–803. https://doi.org/10.1016/j.energy.2019.04.115.

Wei, Y.S., Wang, J.L., Qi, Y.D., Jin, Y.Q., 2018. Optimization of shale gas well pattern and spacing. Nat. Gas. Ind. 38 (4), 129–137 (in Chinese).

Wu, Y.H., Cheng, L.S., Huang, S.J., Xue, Y.C., Ding, G.Y., 2018. A semi-analytical method of production prediction for shale gas wells considering multi-nonlinearity of flow mechanisms. Sci. Sin. Tech. 48, 691–700. https://doi.org/10.1360/N092017-00138.

Xiao, C., Wang, G.D., Zhang, Y.Y., Deng, Y., 2022. Machine-learning-based well production prediction under geological and hydraulic fracture parameters uncertainty for unconventional shale gas reservoirs. J. Nat. Gas Sci. Eng. 106, 104762. https://doi.org/10.1016/j.jngse.2022.104762.

Xiong, J., Lin, H.Y., Li, Y.J., Yan, S., Liu, X.J., He, H.M., Zheng, S., Hu, D., 2022. The desorption laws of different minerals in the organic-rich shale. Acta Pet. Sin. 43 (7), 989–997 (in Chinese).

Xu, Y.J., Liu, Q.G., Li, X.P., Meng, Z., Yang, S.H., Tan, X.H., 2021. Pressure transient and Blasingame production decline analysis of hydraulic fractured well with induced fractures in composite shale gas reservoirs. J. Nat. Gas Sci. Eng. 94, 104058. https://doi.org/10.1016/j.jngse.2021.104058.

Zhang, F.Y., Meybodi, H.E., 2020. A Semianalytical method for two-phase flowback rate-transient analysis in shale gas reservoirs. SPE J. 25 (4), 1599–1622. https://doi.org/10.2118/201225-PA.

Zeng, J., Liu, J.S., Li, W., Leong, Y.K., Elsworth, D., Guo, J.C., 2021. Shale gas reservoir modeling and production evaluation considering complex gas transport mechanisms and dispersed distribution of kerogen. Petrol. Sci. 18 (1), 195–218. https://doi.org/10.1007/s12182-020-00495-1.